JAMES | Journal of Advances in Modeling Earth Systems

RESEARCH ARTICLE
10.1029/2018MS001506

Evaluation of FAMIL2 in Simulating the Climatology and Seasonal-to-Interannual Variability of Tropical Cyclone Characteristics

Jinxiao Li[1,2,3], Qing Bao[1,2], Yimin Liu[1,2,3], Guoxiong Wu[1,3], Lei Wang[1,3], Bian He[1,2], Xiaocong Wang[1,2], and Jiandong Li[1]

[1]State Key Laboratory of Numerical Modeling for Atmospheric Sciences and Geophysical Fluid Dynamics (LASG), Institute of Atmospheric Physics, Chinese Academy of Sciences, Beijing, China, [2]CAS Center for Excellence in Tibetan Plateau Earth Sciences, Chinese Academy of Sciences (CAS), Beijing, China, [3]College of Earth and Planetary Sciences, University of Chinese Academy of Science, Beijing, China

Key Points:
- Characteristics of global and regional tropical cyclone are simulated in FAMIL2
- We identify potential reasons to tropical cyclone activity in FAMIL2
- We discuss the impacts of spatial resolution and introduce the application development of tropical cyclone prediction

Correspondence to:
Q. Bao and Y. Liu,
baoqing@mail.iap.ac.cn;
lym@lasg.iap.ac.cn

Citation:
Li, J., Bao, Q., Liu, Y., Wu, G., Wang, L., He, B., et al. (2019). Evaluation of FAMIL2 in simulating the climatology and seasonal-to-interannual variability of tropical cyclone characteristics. *Journal of Advances in Modeling Earth Systems*, *11*, 1117–1136. https://doi.org/10.1029/2018MS001506

Received 20 SEP 2018
Accepted 18 MAR 2019
Accepted article online 20 MAR 2019
Published online 30 APR 2019

Abstract We evaluate the ability of the latest generation atmospheric general circulation model from State Key Laboratory of Numerical Modeling for Atmospheric Sciences and Geophysical Fluid Dynamics, Institute of Atmospheric Physics, Chinese Academy of Sciences (namely, FAMIL2) in simulating some key characteristics (genesis location, track, number, and intensity) of tropical cyclones (TCs) in terms of their climatology and seasonal to interannual variability. A standard 1° × 1° atmospheric model intercomparison project experiment is carried out for the period 1979–2002, and the last 20 years of outputs are used for analysis. The same period from International Best Track Archive for Climate Stewardship (IBTrACS) is used as the observation for comparison purposes. The evaluations focus on TC activity at the global scale as well as in the three key regions of the northern Indian Ocean (NIO), western Pacific (WP) and northern Atlantic (NA). With respect to the simulated TC climatology, FAMIL2 shows notable ability in correctly reproducing the main characteristics of the genesis locations, tracks, and numbers of TC, particularly over the key regions of TC activity in the Northern Hemisphere; whereas, it underestimates the intensities of TC, as is the case with many state-of-the-art climate models operating at a medium resolution. On seasonal-to-interannual time scales, meanwhile, FAMIL2 successfully reproduces the seasonal cycles of TC numbers over the NIO and WP regions, the former being characterized by double TC peaks (in May and October) and the latter by a maximum peak season in August. However, the model only captures these features approximately. For the simulated interannual variability of TC activity, the correlation coefficients of 20-year TC numbers between FAMIL2 and IBTrACS are 0.22, 0.51 (95% confidence interval), and 0.49 (95% confidence interval) for the NIO, WP, and NA, respectively. We also examine the possible reasons behind the performance of FAMIL2 by investigating its subseasonal signs related to the Madden-Julian Oscillation (MJO) and convectively coupled equatorial waves. The TC genesis potential index is employed to investigate the possible impacts of the large-scale dynamic fields on the simulation of TC activity. Finally, the biases of simulated TC activity, as well as possible solutions for these biases, are discussed with respect to the horizontal resolution of the model. A TC forecasting case study is introduced as a first step in applying FAMIL2 to a TC forecasting system.

1. Introduction

Tropical cyclones (TCs), as one of the most drastic phenomena on the synoptic scale, are accompanied by a warm core, strong vorticity, extreme rainfall, and high wind speeds. Although all such systems form over the tropical oceans, they often go on to have serious adverse impacts on human life when making landfall and hitting our cities (Emanuel, 2005). A reliable estimation indicates that losses attributable to TCs amounted to around $700 billion from 1971 to 2016 (Emanuel, 2017). Then, in 2017, these losses grew by a further $284.7 billion (CRED, 2018). Moreover, this number is expected to increase in the future compared to baseline conditions (Mendelsohn et al., 2012). There have been two main avenues of research regarding TC. On the one hand, researchers have focused on the variation of TC in different basins with respect to global climate changes; for example, the future projection of variations in TC numbers and intensity (e.g., Knutson et al., 2010; Murakami et al., 2011, 2012). On the other hand, predicting TC activity from synoptic to extended-range time scales by using a high-resolution coupled prediction system has emerged as a popular

approach and shown promise in improving the prediction skill and understanding of TCs in recent years (e.g., MacLachlan et al., 2015; Manganello et al., 2016; Murakami et al., 2016). Emanuel (2017) pointed out that strong and fast hurricanes appearing more frequently (e.g., Hurricane Sandy, which formed in the northern Atlantic (NA) in October 2012) represents a huge challenge for TC forecasting, with most models unable to predict the tracks of such TC very well (Xiang, Lin, et al., 2015). Therefore, there is considerable value in improving model performance with respect to TC, from the point view of not only long-term projection but also short-term forecasting.

There is, however, evidence that state-of-the-art global climate models with a relatively higher horizontal resolution have a greater ability to capture TC activities realistically. Previous studies (e.g., Bender, Ginis, et al., 1993; Bender, Ross, et al., 1993; Haarsma et al., 1993) have pointed out that accurately describing TC is limited by incomplete parameterizations and large climatic biases. Fortunately, with the development of high-performance computing and the models themselves, we can now handle synoptic-scale phenomena more reasonably in these higher-resolution models, by which we mean horizontal resolutions from 100 to 25 km or even higher (e.g., Caron et al., 2011; Manganello et al., 2012; Murakami et al., 2011; Oouchi et al., 2006; Zhao et al., 2009). However, alongside these developments, atmospheric general circulation models (AGCMs) are another effective tool to investigate the performance in simulating TC at high resolution (Chen & Lin, 2013; Zhao et al., 2009), as compared to fully coupled general circulation models (Small et al., 2014). Indeed, there are many international projects whose aim is to compare the performance of AGCM in simulating TC under high-resolution conditions (e.g., Shaevitz et al., 2014). For example, the U.S. CLIVAR Hurricane Working Group (Walsh et al., 2015) focuses on assessing the performance of multiple high-resolution American models in simulating TC. This project uses the same rules in terms of forcing and time scales and thus can compare model performances in a fair way. Generally, although there are deficiencies in their TC simulations, high-resolution models can describe many aspects of TC, such as their climatology, interannual variability, and intensity.

Of course, ultrahigh resolution models are the ultimate aim in terms of TC simulation and real-time prediction. But there are currently huge drawbacks in this respect, such as the computational expense and power required, as well as data storage issues. Furthermore, these problems are worse still when an ensemble approach is involved. One solution might be to use regional climate models, since these have the potential to deliver ultrahigh resolution modeling more easily to studies of TC activity. However, there are many advantages for TC forecasting in using global-scale high-resolution modeling, rather than regional modeling. For example, it decreases the dependence on lateral boundary conditions and the sensitivity of physical parameterizations. Furthermore, because the prediction signal beyond the weather time scale may derive from nonlocal and large-scale processes, regional models are limited in terms of to what extent they can improve the lead time of forecasts at longer time scales (e.g., Manganello et al., 2016, 2017; Shen et al., 2017; Shepherd & Walsh, 2016; Xiang, Zhao, et al., 2015). Another method that considers large-scale effects while adopting the high resolution of the regional scale is the nested or stretched grid method (e.g., Harris & Lin, 2014, 2016; Zarzycki & Jablonowski, 2014). In terms of application, on the one hand, it is a good option for establishing a synoptic-to-seasonal-scale forecasting system for global TC activity based on medium-resolution GCMs; while, on the other hand, it is also a good option for establishing a similar system for regional TC activity by using a nested or stretched global grid. In terms of scientific analysis, it is necessary to discuss the simulated TC activity under superhigh resolution conditions. For example, Japanese scientists launched the Global 7-km Mesh Non-hydrostatic Model Intercomparison Project for Improving Typhoon Forecasts (or TYMIP-G7, for short; Nakano et al., 2017). Preliminary results have shown enormous improvement in TC simulation and forecasting by using a nonhydrostatic dynamical core at ultrahigh resolution (<10 km).

In addition to increased horizontal resolution and better representation of physical processes in models, there are many other aspects that can help improve the simulation of TC in GCMs. On the one hand, with improvements in parameterizations, especially moist processes and tropical variabilities (e.g., the Madden-Julian Oscillation (MJO) and convectively coupled equatorial waves (CCEWs)), from the subseasonal to seasonal time scale, can be simulated more reasonably than before (e.g., Hung et al., 2013; Jiang et al., 2013; Lin et al., 2006; Oouchi et al., 2009; Peters et al., 2017). On the other hand, objective feature-tracking methodologies can be used to detect the signals of TC directly (e.g., Bengtsson et al., 2007; Hodges, 1994, 1999; Knutson et al., 2007; Oouchi et al., 2006; Walsh et al., 2007; Wu & Lau, 1992; Zhao et al., 2009) thus

diminishing the biases attributable to illusory signals of TC. Besides, some studies have focused on the parameters and processes that have physical links with TC activity (e.g., Fuentes- Franco et al., 2017; Reed & Jablonowski, 2011a, 2011b; Shepherd & Walsh, 2016; Tao & Zhang, 2014). Zhao et al. (2012) discussed the important role played by physical and dynamic parameters in the simulation of TC. They found that divergence damping and the parameterization of moist convection, in particular, the cumulus mixing rate in the convection scheme of Bretherton et al. (2004), are sensitive to TC frequency in HiRAM (Harris & Lin, 2014; Zhao et al., 2009). NASA's GEOS-5 model produces a similar result (Lim et al., 2015). They found that the time scale of plumes and the minimum entrainment threshold in the Arakawa-Schubert scheme (Arakawa & Schubert, 1974; Moorthi & Suarez, 1992) are sensitive to the ability to simulate TC. These results suggest that if a model's physical processes related to TC activities are reasonable, the characteristics of TC can be captured at a suitable resolution.

FAMIL2 is the latest generation atmospheric model of the State Key Laboratory of Numerical Modeling for Atmospheric Sciences and Geophysical Fluid Dynamics, Institute of Atmospheric Physics, Chinese Academy of Sciences; compared with the former version, SAMIL (Bao et al., 2010, 2013). The dynamical core of FAMIL2 has switched to a finite-volume method (Lin, 2004; Voosen, 2017) and is discretized on a cubed-sphere grid system (Putman & Lin, 2007), which makes it possible to simulate TC activity at a resolution of 100 km to as fine as 6.25 km (Li et al., 2017; Zhou et al., 2012). As the atmospheric component of Climate system model CAS FGOALS-f2/3, the C96 (~100 km) resolution of FAMIL2 will be participating in Coupled Model Intercomparison Project Phase 6 (CMIP6) activities (Eyring et al., 2016). The C384 resolution of FAMIL2 (approximately 25 km) is participating in CMIP6 High Resolution Model Intercomparison Project (HighresMIP; Haarsma et al., 2016), and the performance in simulating TC is considered an important indicator in evaluating high-resolution models. At the first step, simulation and prediction experiments in AGCM FAMIL2 with fixed SST are designed as the exploratory studies. But Emanuel and Sobel (2013) indicated the deficiency in prescribing the SST for realistic TC simulation, which is not beneficial for the maintainance of surface energy balance. Then, a coupled real-time subseasonal-to-seasonal forecasting system has been established recently and operationally used as one member in China multiple model ensemble system (China MME) proposed by Beijing Climate Center.

The purposes of the present study are, by using FAMIL2 at the horizontal resolution of C96 (~100 km), (1) to evaluate its general performance in terms of global- and regional-scale simulation of TC genesis locations, tracks, numbers, and intensity; (2) to compare the global and regional TC numbers with IBTrACS data on the interannual time scale; and (3) to reveal the possible reasons behind the performance of the model in simulating TC activity by investigating the subseaonal variability related to the MJO, CCEWs, and the TC genesis potential index (GPI) calculated through the outputs of FAMIL2. Additionally, results using the higher horizontal resolution and prediction of one typical TC case are also presented.

This paper is structured as follows: Section 2 describes the model, the observational data sets and the design of the numerical experiments. Section 3 introduces the detection method used in this paper. In section 4, results regarding the climatological genesis locations and tracks, interannual variability, and intensity of TC are presented and discussed. Section 5 discusses the possible impacts from the horizontal resolution and reports a prediction skill of FAMIL2 for a specific TC case. Finally, section 6 summarizes the key conclusions of our study and discusses possible future avenues of related research.

2. Model, Data, and Experimental Design

2.1. Model Description

As in version 1 of FAMIL (Zhou et al., 2015), FAMIL2 uses a finite-volume dynamical core (Lin, 2004), and combines this with a flux-form semi-Lagrangian advection scheme (Wang et al., 2013) on a cubed-sphere grid system (Putman & Lin, 2007). The horizontal resolutions of FAMIL2 can vary from C48 (approximately 200 km) to C1536 (approximately 6.25 km) in both AMIP-like runs and a fully coupled run. The number of vertical layers has been increased to 32 from 26, and the atmospheric layers extend from the surface to 1 hPa. The vertical spacing of FAMIL2 is the same as GFDL HiRAM (Zhao et al., 2009). Besides, the main computing platform of FAMIL2 is Tianhe-2, located in Guangzhou, China, which was the fastest supercomputer in the world from June 2013 to May 2016 (https://www.top500.org/). The computational performance of

FAMIL2 in Aqua-Planet Experiments (Zhou et al., 2012) and under AMIP conditions (Li et al., 2017) has been well evaluated.

Compared with FAMIL1, FAMIL2 has replaced the planetary boundary layer scheme, which was a "nonlocal" first-order closure scheme (Holtslag & Boville, 1993), with the University of Washington moist turbulence (UWMT) parameterization (Park & Bretherton, 2009). UWMT is a nonlocal high-order closure scheme and uses diagnosed turbulent kinetic energy to determine the eddy diffusivity in turbulence. Compared to the previous planetary boundary scheme, the UWMT scheme considers turbulence to be affected by all processes that influence the vertical structure, and the results of the UWMT scheme are insensitive to changes in the horizontal or vertical resolution. The microphysical parameterization used in FAMIL2 is a single-moment scheme, which is the revised Lin scheme (Lin et al., 1983). The scheme explicitly treats the mass mixing ratio of six hydrometeor species (water vapor, cloud water, cloud ice, rain, snow, and graupel), which is also used in GFDL HiRAM (Harris & Lin, 2014; Zhao et al., 2009). The land surface model used in FAMIL2 is CLM4.0 (version 4 of the Community Land Model; Oleson et al., 2010), which is coupled with the atmospheric component via the version 7 coupler in CESM (Craig et al., 2012). The frequency of the coupling is 48 times per day, and the processes from the dynamic global vegetation model (DGVM) in CLM4.0 are turned off during the coupling with FAMIL2. Thus, the processes related to carbon biogeochemistry, nitrogen biogeochemistry, and the urban model are fixed in FAMIL2. As in FAMIL2, there are two horizontal resolutions of CLM4.0: 1° nominal resolution for the most CMIP6-endorsed MIPs and 0.25° nominal resolution for CMIP6 HighResMIP. In addition, a resolving convective precipitation parameterization (©2017 FAMIL Development Team) is used, which involves calculating the microphysical processes in the cumulous scheme for both deep and shallow convection, six species are considered similar to the microphysics scheme (Harris & Lin, 2014; Lin et al., 1983). Owing to the quick phase changes within the convective cloud, a subtime step of 150 s is used to calculate the microphysical processes.

2.2. Observational Data

To assess the model results, the IBTrACS (version v03r09) data set (Knapp et al., 2010) is used as a comparison, which the data sources are derived from many agencies. For example, the best track data set in Western Pacific Basin comes from RSMC Tokyo and CMA-Shanghai Typhoon Institute (Ying et al., 2014). The 10-min-averaged wind speed at an elevation of 10 m for the maximum sustained wind is regarded as the observed wind speed and is corrected to 1 min in order to compare to model's outputs directly. The conversion coefficient is set to 0.88, and the threshold of a tropical storm is set from 18.01 m/s to 15.84 m/s (Knapp et al., 2010; Manganello et al., 2012). Tropical depressions whose wind speeds are lower than 15.84 m/s during their entire life cycle are filtered to highlight strong TC events.

OISSTv2 (Banzon et al., 2016; Reynolds et al., 2007) data during 1983–2002 are used to prescribe the SST for FAMIL2. The TRMM 3B42 (https://trmm.gsfc.nasa.gov/) data for the period 2001–2010 along with ERA-Interim data (Dee et al., 2011) are used to evaluate the performance of FAMIL2 in simulating the tropical cyclone GPI, MJO, and CCEWs.

2.3. Experimental Design

A 20-year (1983–2002) AMIP-like (Gates, 1992) run is designed to evaluate the global- and regional-scale TC activity. The forcing data used to drive FAMIL2 are as follows: daily SST data from OISSTv2; the solar constant (Hartmann, 1994); greenhouse gas and ozone forcing data (Meinshausen et al., 2011); and five types of three-dimensional aerosols (Lamarque et al., 2012). The physical time steps are set to 30 min, and then variables including the surface wind, sea level pressure, absolute vorticity, and temperature are output every 6 hr.

3. TC Detection and Tracking Method

Different to the more traditional method that uses several parameters to represent TC, we use an objective feature-tracking approach (Tables 1–3). The identification criteria (Table 3) conform to the Saffir-Simpson (SS) intensity scale (Table 1) and Chinese intensity scale (Table 2). Also, the structure of the package is similar to the TSTORM software (https://www.gfdl.noaa.gov/tstorms/), designed to detect TC in HiRAM (Zhao et al., 2009) and HiFLOR (Murakami et al., 2016). Weak and short-lived TC has been filtered out from the model results. Considering that the model time step is 30 min, compared to 1 min for the IBTrACS, the

Table 1
The Saffir-Simpson (SS) Intensity Scale

SS category	Wind speed (m/s)
Tropical storm	>17.4 and ≤32.3
Category 1	>32.3 and ≤42.1
Category 2	>42.1 and ≤48.8
Category 3	>48.8 and ≤57.5
Category 4	>57.5 and ≤69.3
Category 5	≥69.3

surface wind of the model's lowest level (~60 m) should be corrected to 10 m based on 0.88 as the conversion coefficient (Knapp et al., 2010). The wind speed threshold is consistent with a recent study on the relationship between a model's horizontal resolution and the TC detection algorithms (Walsh et al., 2007).

The TC detection algorithm has been developed and modified based on the work of Knutson et al. (2007) and Zhao et al. (2009). Our detection algorithm consists mainly of three modules:

1. *Potential TC identification at each grid point*: Six-hourly model outputs are used for TC identification. At each time, cases where the 850-hPa absolute vorticity is greater than 3.5×10^{-5} within the 600 km × 600 km grid box will be picked out. To confirm the center of the TC, there must be a grid point sea level pressure minimum within a 2° × 2° grid box that centers on the grid point vorticity maximum. Besides, there must be a warm core defined as the average temperature between 300 and 500 hPa in the center of the TC that is 1 °C warmer than another grid point within the surrounding 2° × 2° grid box.
2. *TC track identification*: When the TC identification module has completed, the TC track module will judge if there is a continuous TC event. By using the location of the TC center at the present time, the module will check if any TC appears in the 5° × 5° grid box in the next 6-hr period. If the module cannot find a suitable TC, the TC event is terminated. If there is more than one TC event in the 5° × 5° grid box, the closest one is chosen as the successive TC from the last 6-hr period. To filter out short-lived TC (Knutson et al., 2007; Shaevitz et al., 2014; Walsh et al., 2007; Zhao et al., 2009), the maximum surface wind speed of TC must be greater than 15.84 m/s, and the lifetime of the TC must be greater than 72 hr (3 days).
3. *Classifying the TC*: The intensity of TC is categorized using the modified SS scale (Simpson & Saffir, 1974; Table 2). Then, it is divided into seven parts of the global basin in accordance with IBTrACS (Figure 1). A statistic for the TC number in each month is designed for analyzing the seasonal cycle.

4. Results

4.1. Global Climatology of TC Density, Track, and Numbers

The genesis locations of TC simulated by FAMIL2 at C96 (~100 km) are shown in Figure 2b. For comparison, the results of IBTrACS are also shown in Figure 2a. We can see that FAMIL2 at this horizontal resolution can prescribe the genesis location of TC reasonably. Most locations of TC are concentrated over regions where the $V_{\max}$ is greater than 50 m/s (Emanuel, 1987; Korty et al., 2012; Royer et al., 1998), which is the dynamic basis for TC genesis (thick contour).

The $V_{\max}$ (the maximum potential intensity) used in this paper is defined as

$$V_{\max} = \frac{C_k T_s}{C_d T_0}\left(CAPE^{*} - CAPE^{b}\right), \tag{1}$$

where C_k is the exchange coefficient of enthalpy, C_d is the drag coefficient, T_s is the SST, and T_0 is the mean outflow temperature. $CAPE^{*}$ is the convective available potential energy (CAPE) of the air lifted from saturation at sea level, and $CAPE^{b}$ is the CAPE of the boundary layer air (Emanuel, 1995).

Table 2
The Chinese Typhoon Intensity Scale

Typhoon category	Wind speed (m/s)
Tropical storm	>17.1 and ≤24.4
Strong tropical storm	>24.4 and ≤32.6
Typhoon	>32.6 and ≤41.4
Strong typhoon	>41.4 and ≤50.9
Super typhoon	≥50.9

In the western Pacific (WP) basin, most TC occur to the south of 30°N. Compared to IBTrACS, more TC occur between 10°N and 20°N. In the NIO, compared to IBTrACS, more TC occur near the coast in the northern Indian Ocean (NIO). In the Northern Atlantic (NA), the total number of TC is lower than that of IBTrACS, and the primary bias appears in the nearshore area of Northwest Africa. Similarly, the global tracks of TC simulated by FAMIL2 are shown in Figure 3b, with the results from IBTrACS in Figure 3a for comparison and the TC in the NIO, WP, and NA shown separately. Compared to IBTrACS, the TC in the NIO simulated by FAMIL2 are similar; whereas, in the WP, the number of tracks

Table 3
TC Identification Criteria in FAMIL2

Variables	Threshold
Surface wind speed threshold (m/s)	≥14.0
850-hPa absolute vorticity (s^{-1})	3.5×10^{-5}
Warm core (averaged temperature between 300 and 500 hPa; K)	1
Life time (h)	72

at lower latitudes is reasonable but more than that observed at the eastern part of 160°E. In the NA, the number of tracks is less than that observed to some extent.

Figure 4 compares the number of TC in each basin in percentage terms (TC percentage). The model shows good performances over the northern Atlantic (NA), southern Indian Ocean (SI), and Northern Indian Ocean (NI). The primary bias in the TC percentage appears in the Eastern Pacific (EP), being only 6.7% in the simulation but 20.5% in the IBTrACS. Another major bias appears in the WP, with 42.1% in the simulation but 31.7% in the IBTrACS. The negative bias of the number of TC in the EP could be a common problem compared with other AGCMs (Manganello et al., 2012; Zhao et al., 2009).

Figure 5 shows the seasonal cycle of TC in the NIO, WP, and NA. The results simulated by FAMIL2 is close to the IBTrACS, and compared to the results of HiRAM (Zhao et al., 2009) the peak in TC numbers can be described reasonably in both the NIO and WP. In the NIO, the seasonal cycle of TC numbers shows a double-peak pattern, with two active seasons of TC activity. The first peak is from April to June and the second from September to December. In the simulation, the results for TC numbers in the first active season are close those in the IBTrACS; however, a large bias appears in the second active season, especially in November, when the number of TC is underestimated. In the WP, the seasonal cycle of TC numbers shows a single-peak pattern. Specifically, the active TC season in the WP is from June to November, when there are usually more than two TC geneses, and the maximum number of TC is in August, which can reach up to about eight. In the simulation, the TC numbers in the active season (June to November) and inactive season (December to April) are close to those in the IBTrACS. The primary bias appears in the transitional season (April to June). Especially in May, FAMIL2 underestimates by about one TC in the WP—a bias that may reflect a general deficiency of FAMIL2 during seasonal transition (spring to summer) in the WP. The shape for the seasonal cycle of TC activity in the NA is similar to the result in the WP. A single-peak pattern is apparent but with the maximum number of TC appearing in September. Although the simulated results for TC numbers are close to those of the IBTrACS during the inactive season (December to May) and transitional season (May to July), large bias appears in the active season (July to November), during which only around 60% of TC (approximately five in IBTrACS and three in FAMIL2) activity in the NA can be captured.

4.2. Global Climatology of TC Intensity

Figure 6 shows the tracks of TC and their variation in intensity. TC in both the simulation of FAMIL2 and observation of IBTrACS are grouped into seven categories in accordance with the modified SS scale (Table 2), but only show the TC which intensities are stronger than "tropical storm" (TS). From the global perspective, the intensity of TC is concentrated from TS to "category 3". In the NIO, because severe TC are relatively rare, the intensity simulated by FAMIL2 is close to that in IBTrACS. In the WP (Figure 6b) and in the NA (Figure 6c), the distribution of TC intensity simulated by FAMIL2 is narrower than that in the IBTrACS. Zarzycki and Jablonowski (2014) used CAM-SE to do the TC simulation at nearly 100-km horizontal resolution. The result of TC intensity in CAM-SE is similar to the result in FAMIL2. Although more TC events are simulated in FAMIL2 than CAM-SE, it is difficult to reproduce the intensity of TC with the coarse resolution.

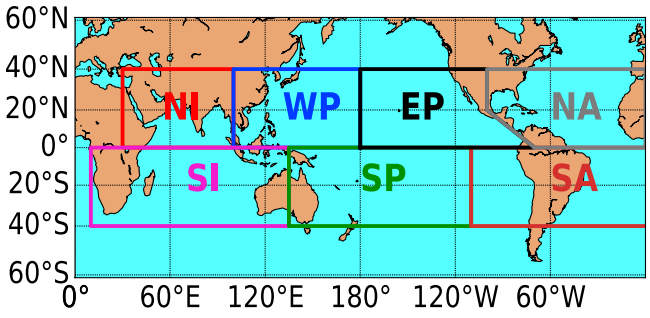

Figure 1. The seven basins in FAMIL2: Northern Indian Ocean (NI, red box); western Pacific Ocean (WP, blue box); eastern Pacific Ocean (EP, black box); northern Atlantic Ocean (NA, gray box); southern Indian Ocean (SI, purple box); southern Pacific Ocean (SP, green box); and southern Atlantic Ocean (SA, brown box). The division conforms with that in the IBTrACS data set.

Figure 7 shows the pressure–wind relationship between the results of TC simulated by FAMIL2 and those in IBTrACS. Each point refers to a relationship between 6-hr surface pressure and 6-hr 10-m wind (simulation in blue; IBTrACS in red). The left-hand side of each plot is the low surface pressure and high 10-m wind speed area, which is reflective of severe TC. The results are similar to those of Figure 6; the TCs are concentrated in the midintensity position. In the NIO (Figure 7a), WP (Figure 7b), and in the NA (Figure 7c), there are fewer TC, for which the 10-m speeds are more than 40 m/s and the sea level pressure less than 920 hPa. The results indicate that even

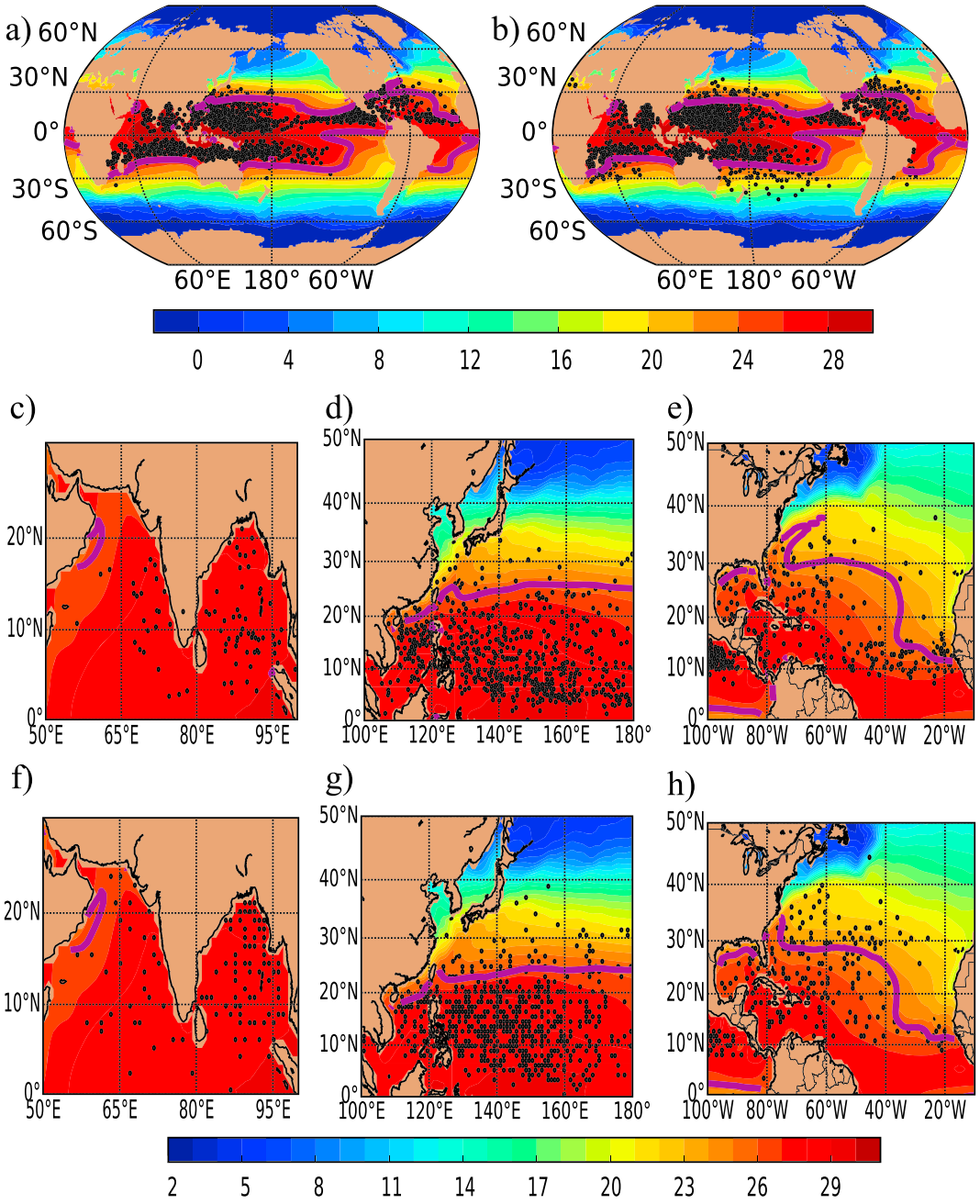

Figure 2. The position of annual tropical cyclone (TC) genesis (black points), which are picked up by using an objective feature-tracking approach and that covered by 20-year-averaged sea surface temperature (shaded). The thick line means the Vmax is greater than 50 m/s, which is the required threshold for TC formation in the current climate (Emanuel, 1987; Korty et al., 2012; Royer et al., 1998). A total of 20 years of data are used here. However, only those TC with lifetimes of at least 3 days are shown, both in International Best Track Archive for Climate Stewardship (IBTrACS, a) and the C96 (~100 km) resolution simulation of FAMIL2 (b). The northern Indian Ocean (c is the result of IBTrACS, f is the result of FAMIL2), western Pacific (d is the result of IBTrACS, g is the result of FAMIL2), and northern Atlantic (e is the result of IBTrACS, h is the result of FAMIL2) basins are also shown.

when FAMIL2 can capture the genesis location and number of TC reasonably, these TCs do not always develop into strong events.

4.3. Interannual Variability of TC Numbers

Figure 8 shows the interannual variability of TC numbers simulated by FAMIL2 (red lines), and observation of IBTrACS (black lines) in the NIO (Figure 8a), WP (Figure 8b), and NA (Figure 8c). Although the numbers

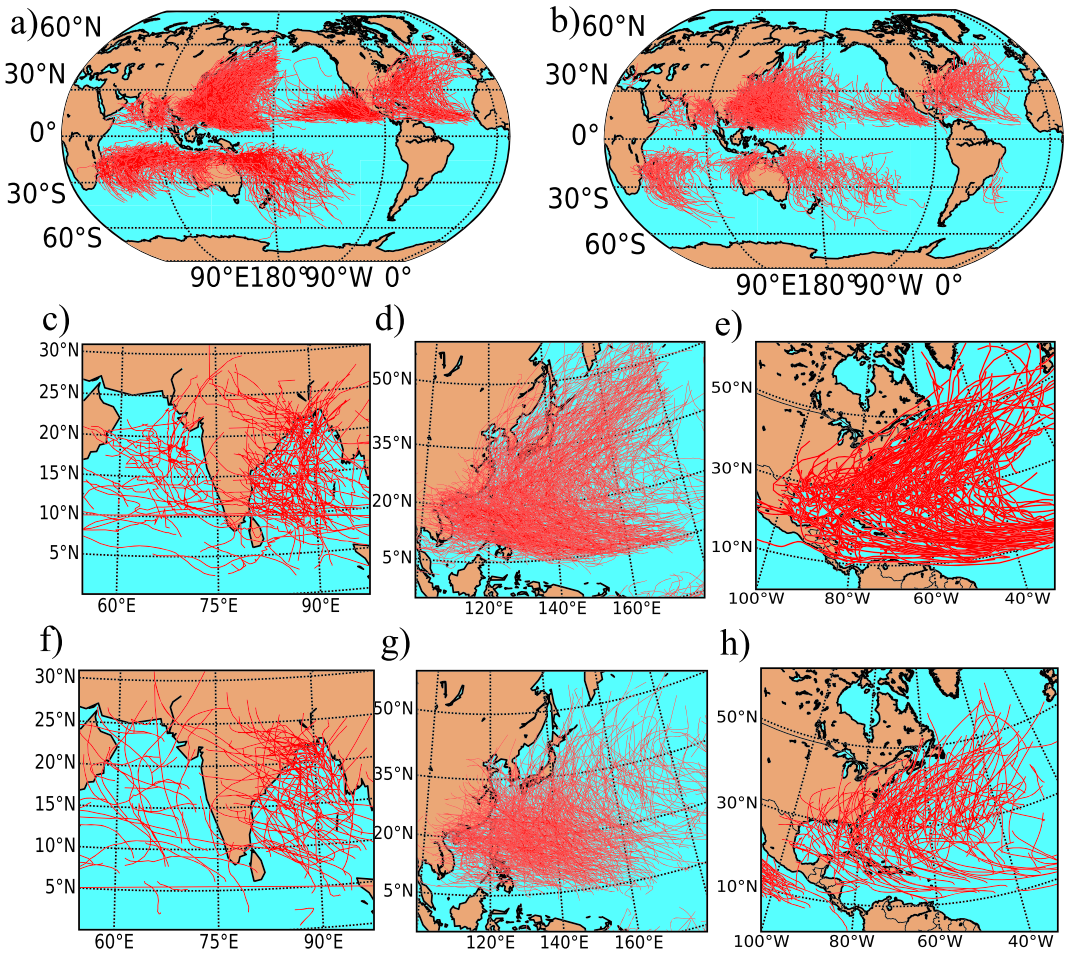

Figure 3. Comparison of observed (a) and model-simulated (b) TC tracks, which are picked up by using an objective feature-tracking approach (resolution: ~100 km; red lines) from 1983 to 2002. Only those TC with a lifetime exceeding 3 days are shown. The northern Indian Ocean (c is the result of International Best Track Archive for Climate Stewardship, IBTrACS, f is the result of FAMIL2), western Pacific (d is the result of IBTrACS, g is the result of FAMIL2), and northern Atlantic (e is the result of IBTrACS, h is the result of FAMIL2) basins are also shown.

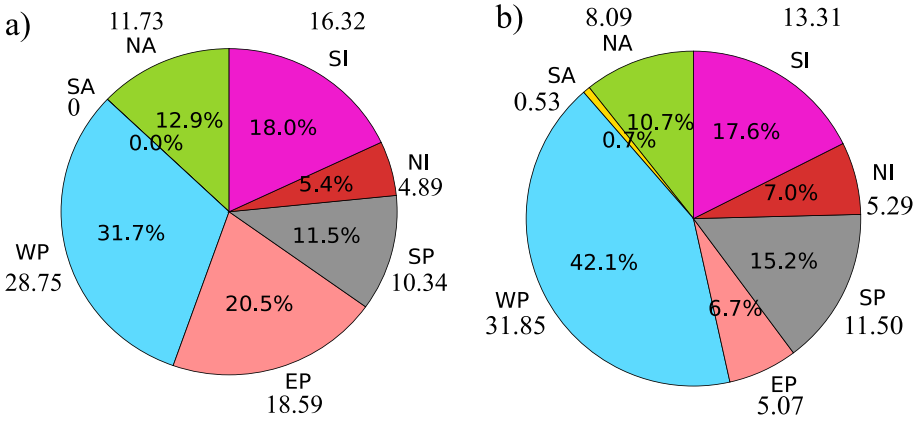

Figure 4. Comparison of the number of tropical cyclone in each basin in percentage terms between (a) IBTrACS and (b) FAMIL2 in C96 simulation (~100 km) in the western Pacific (WP, blue), eastern Pacific (EP, pink), southern Pacific (SP, gray), northern Indian Ocean (NI, red), southern Indian Ocean (SI, purple), northern Atlantic (NA, green), and southern Atlantic (SA, yellow). The annually averaged tropical cyclone numbers are also shown in all basin. IBTrACS = International Best Track Archive for Climate Stewardship.

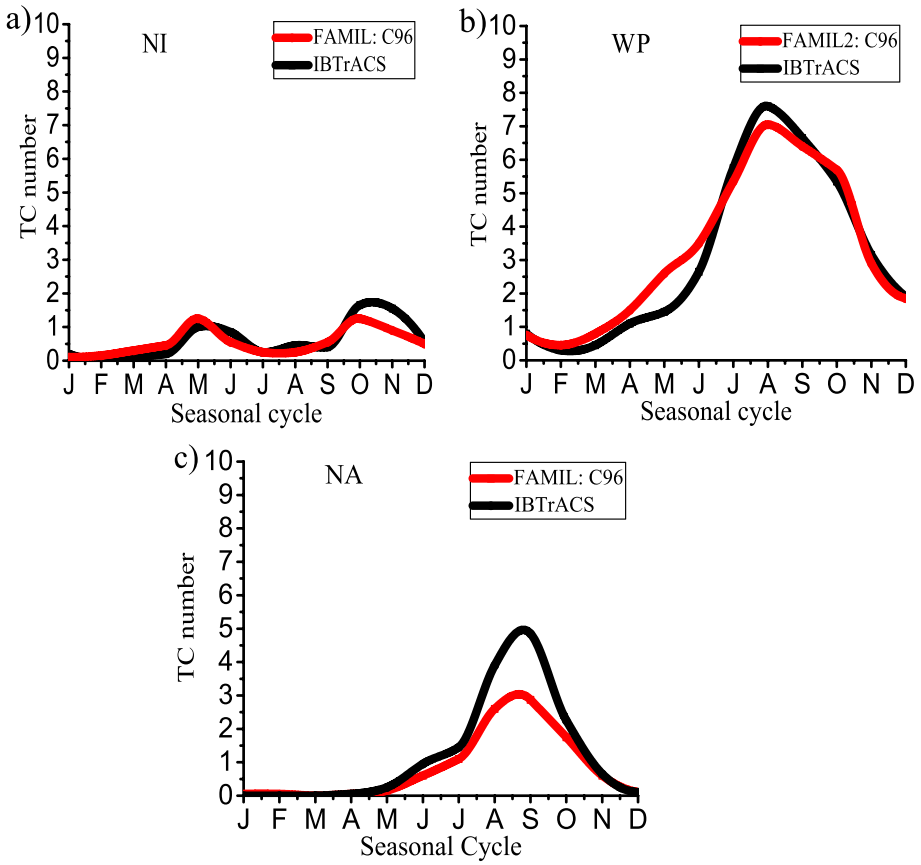

Figure 5. The 20-year seasonal cycle (January–November) of tropical cyclone numbers in the northern Indian Ocean (a), western Pacific Ocean (b), and northern Atlantic (c). The results of FAMIL2 in C96 (~100 km) simulation are shown as red lines, and the results of IBTrACS are shown as black lines. The time periods of the FAMIL2 simulation and IBTrACS are both from 1983 to 2002. IBTrACS = International Best Track Archive for Climate Stewardship.

of TC in the NIO are close to those in IBTrACS, the correlation coefficient between simulation and observation is 0.22. This reflects the difficulties in simulating the interannual variability of TCs in the NIO despite the simulated numbers being close to those observed. The correlation coefficient of the number of TC in the WP reaches 0.51 (95% confidence interval). Several studies (e.g., Manganello et al., 2012, 2017) have pointed out a strong correlation between El Nino–Southern Oscillation (ENSO) and TC activity in the WP. Therefore, the high correlation of TC numbers in the WP may indicate that FAMIL2 well reproduce the possible linkage between TC genesis and interannual variability of SST in the WP. Although the simulated climatological number of TC in the NA is less than that in IBTrACS, the simulated interannual variability of TC number is close to the IBTrACS, and the correlation coefficient of the TC number between simulation of FAMIL2 and observation from IBTrACS in the NA is 0.49 (95% confidence interval). As well as in the WP, the possible linkages of TC genensis and interannual variability of SST in the NA is also captured in these regions to some extent. As Figure 2 shows, the negative bias in TC numbers appears in the eastern part of the NA near the northwest of Africa. The high correlation in annual TC numbers between the simulation and IBTrACS in the WP and NA indicates the potential ability as for the application of the seasonal forecast of TC.

5. Possible Reasons for FAMIL2's Performance in Simulating TC

5.1. Large-Scale Environmental Factors

We use the theory of tropical cyclone GPI developed by Emanuel and Nolan (2004) to investigate the rationality of certain environmental variabilities contributing to the genesis of TC. Camargo et al. (2007) discussed

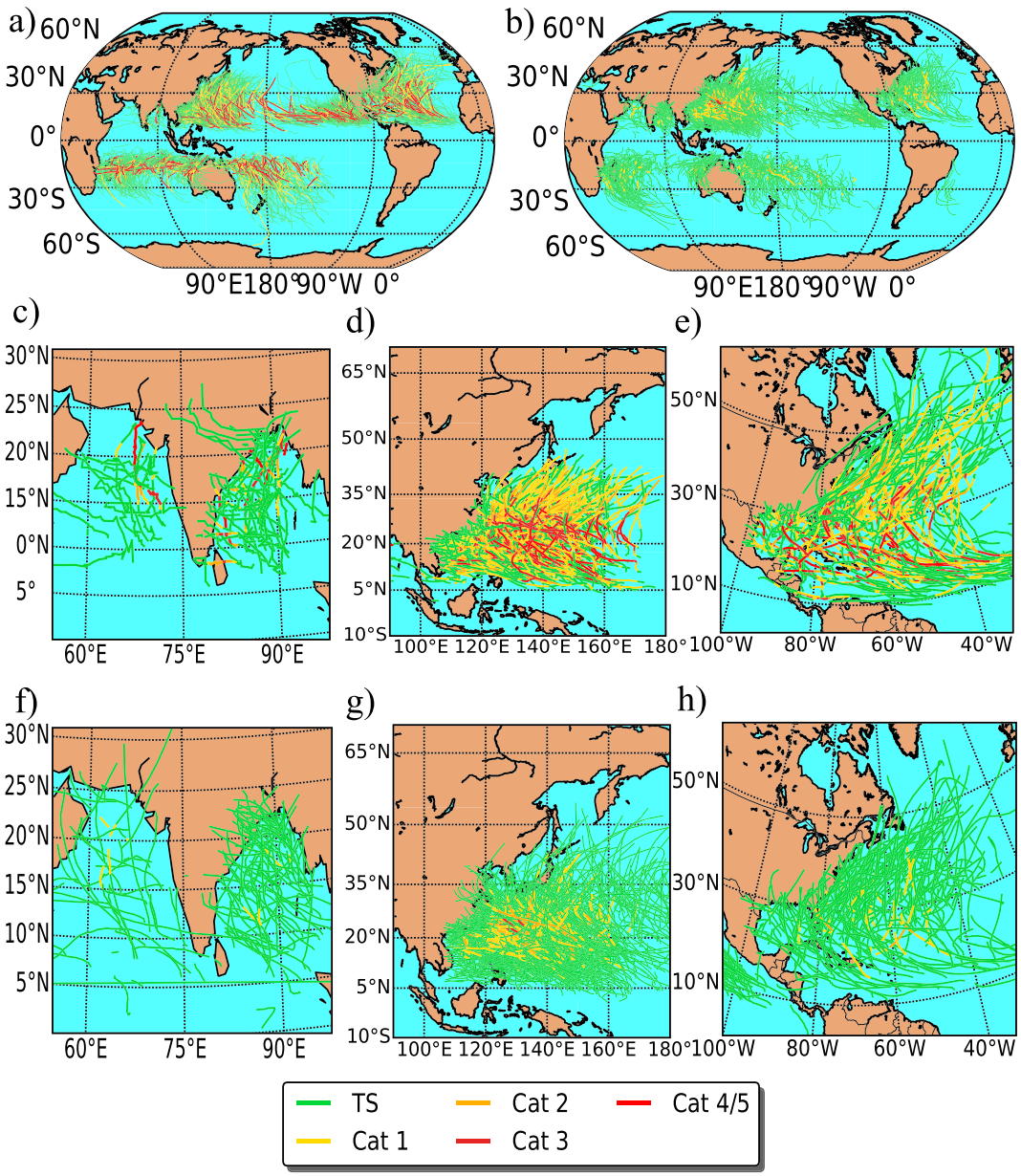

Figure 6. Tropical cyclone (TC) tracks (lines) and intensity (colors): (a) from a 20-year segment (1983–2002) of IBTrACS, and (b) from the simulation of FAMIL2, which are picked up by using an objective feature-tracking approach at the C96 (~100 km) resolution for 1983–2002. Only those TC with a lifetime exceeding 3 days are shown. The TC in both the simulation of FAMIL2 and observation of IBTrACS are grouped into seven categories in accordance with the modified SS scale (Table 2) but only show the TC which intensities are stronger than "tropical storm" (TS). The results between FAMIL2 (f–h) and IBTrACS (c–e) in the northern Indian Ocean (c is the result of IBTrACS, f is the result of FAMIL2), western Pacific (d is the result of IBTrACS, g is the result of FAMIL2), northern Atlantic (e is the result of IBTrACS, h is the result of FAMIL2) basins are also shown. IBTrACS = International Best Track Archive for Climate Stewardship.

the detail of the GPI and used it to diagnose global and regional aspects of TC activity in CMIP5 models. The GPI used in this paper is defined as

$$GPI = \left|10^5 \mathrm{vort850}\right|^{3/2} \left(\frac{RH}{50}\right) \left(\frac{V_{\max}}{70}\right) (1 + 0.1 V_{\mathrm{shear}})^{-2}, \tag{2}$$

where vort850 is the 850-hPa absolute vorticity (s^{-1}), RH is the 600-hPa relative humidity (%), $V_{\max}$ is the maximum potential intensity, V_{shear} is the magnitude of the wind shear between 850 and 200 hPa (m/s).

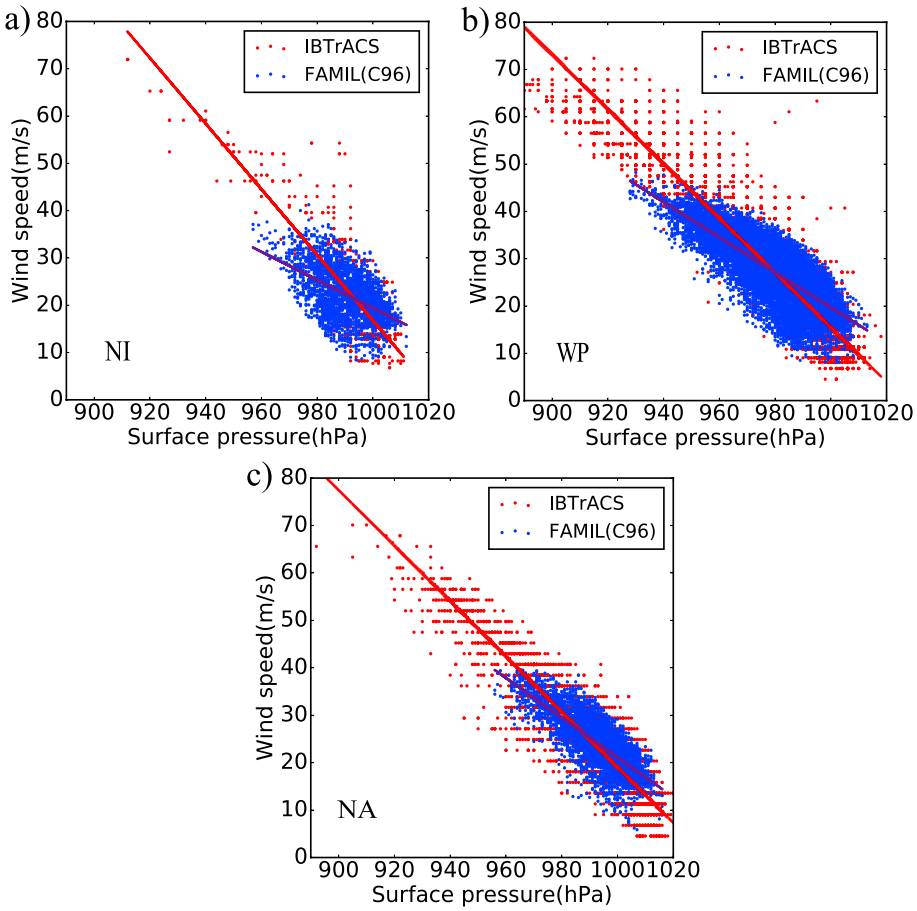

Figure 7. Pressure-wind pairs for each 6-hourly TC measurement for the FAMIL2 in C96 (~100 km) simulation (blue dots) and IBTrACS (red dots) in the western Pacific (a), northern Indian Ocean (b), and northern Atlantic (c). A linear regression (blue line for the result of FAMIL2, red line for the result of IBTrACS) is fitted to each distribution of pressure–wind pairs. IBTrACS = International Best Track Archive for Climate Stewardship.

The GPI establishes the link between the large-scale environmental conditions and TC formation. Figures 9a and 9b show the climatological distribution of the GPI in the simulation by FAMIL2 (Figure 9b) and in ERA-Interim data (Figure 9a) averaged from May to November, which is the primary TC season in the Northern Hemisphere. The results show fundamentally consistent patterns of GPI between ERA-Interim and the simulation by FAMIL2. Thus, the environmental conditions of FAMIL2 for TC genesis are close to those observed. There are biases in the quantitative values of the GPI, which are consistent with the results of the genesis location biases and numbers of TC using the objective feature-tracking methodology in each basin. The GPI values in the NIO and WP are close to those observed, but the values in the EP and NA are less than those observed. To analyze the contribution of the GPI's biases, we calculate the relative bias for each term of the climatological GPI (averaged from May to November) in the NIO, WP, EP, and NA (Figure 9c). On the one hand, the result shows negative biases of $V_{\max}$ in the WP, EP, and NA, and this result is consistent with the intensity of TC detected by the objective feature-tracking methodology. On the other hand, the relative humidity (RH) and wind shear (Wind_shear) show positive biases in the WP, EP, and NA. The moister profile of RH and stronger wind shear go against the genesis conditions necessary for TC, and that is one reason why the number of TC is less than IBTrACS in these basins. Camargo et al. (2007) have discussed the GPI in several climate models. They show positive biases of RH in ECHAM3, ECHAM4, ECHAM5, CCM3, and NSIPP, which are similar to the results of FAMIL2. But the negative biases of wind shear that existed in ECHAM4, ECHAM5, NSIPP are different from the results of FAMIL2.

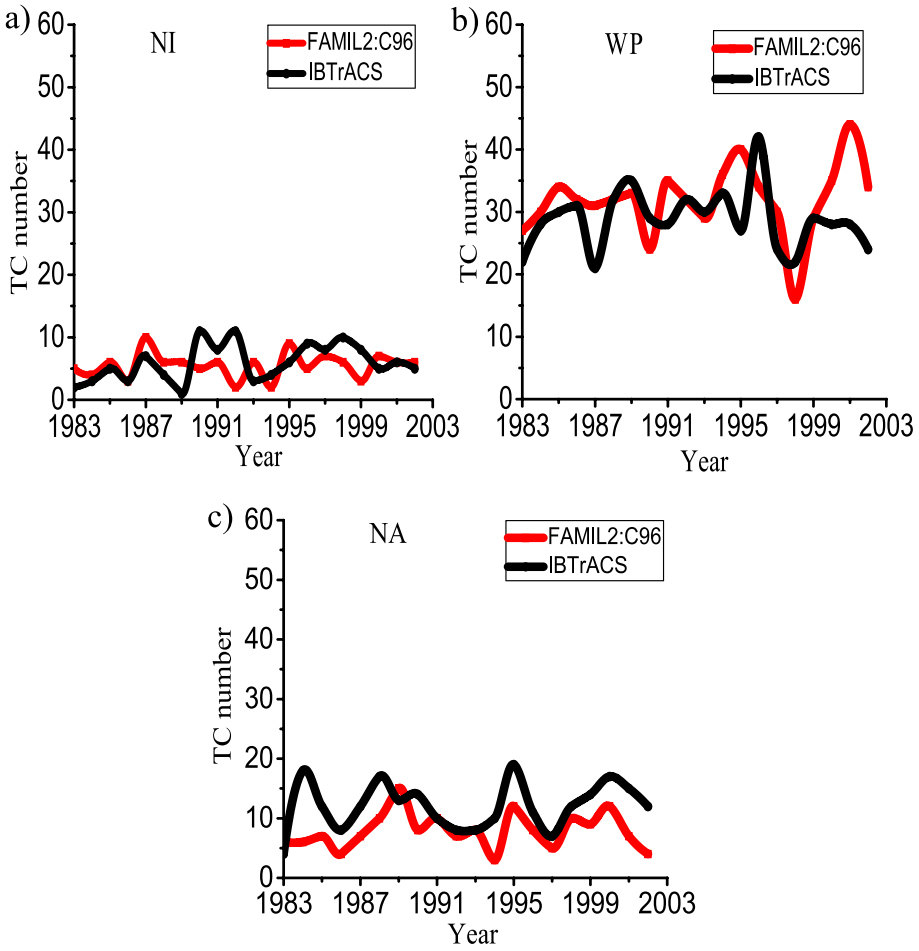

Figure 8. Interannual variation of tropical cyclone (TC) numbers in the (a) northern Indian Ocean, (b) western Pacific Ocean (WP), and (c) northern Atlantic (NA) basins. The results of FAMIL2 in C96 (~100 km) simulation are shown as red lines, and the results of IBTrACS as black lines. The time periods of the FAMIL2 simulation (~100 km) and IBTrACS are both from 1983 to 2002. The correlation coefficients of 20-year TC numbers between FAMIL2 and IBTrACS are 0.22, 0.51 (95% confidence interval), and 0.49 (95% confidence interval) for the NIO, WP, and NA, respectively. IBTrACS = International Best Track Archive for Climate Stewardship.

5.2. The MJO and CCEWs in FAMIL2

Previous studies reveal that the MJO and CCEWs are the prominent intraseasonal variabilities in the tropics (e.g., Wheeler & Kiladis, 2010). Zhang (2005, 2013) discussed the relationship between the MJO and global TC genesis locations and tracks, including its impacts on them. A realistic simulation of the MJO and CCEWs will provide reasonable backgrounds for the simulation of TC (Hung et al., 2013; Waliser et al., 2009).

Figure 10 is an annual (January–December) time-longitude diagrams for lag-composites of precipitation correlated against precipitation in the NIO, along with the 850-hPa zonal winds, in the FAMIL2 simulation (Figure 10a) and observation (Figure 10b). By using 20- to 100-day band-pass filtered data, the MJO's eastward phase is shown. The lag of the zonal wind anomaly behind the precipitation anomaly is about 5–7 days, which is close to that observed. Although the 850-hPa wind speed of FAMIL2 is close to that observed in the western hemisphere, there is the faster eastward propagation of 850-hPa winds in the eastern hemisphere compared observation.

Figure 11 shows the symmetric (observation: Figure 11a; simulation: Figure 11b) and antisymmetric (observation: Figure 11c; simulation: Figure 11d) raw spectra, which have been deducted the background spectra. Persian curves distinguish the prominent area of Kelvin, equatorial Rossby, eastward interior

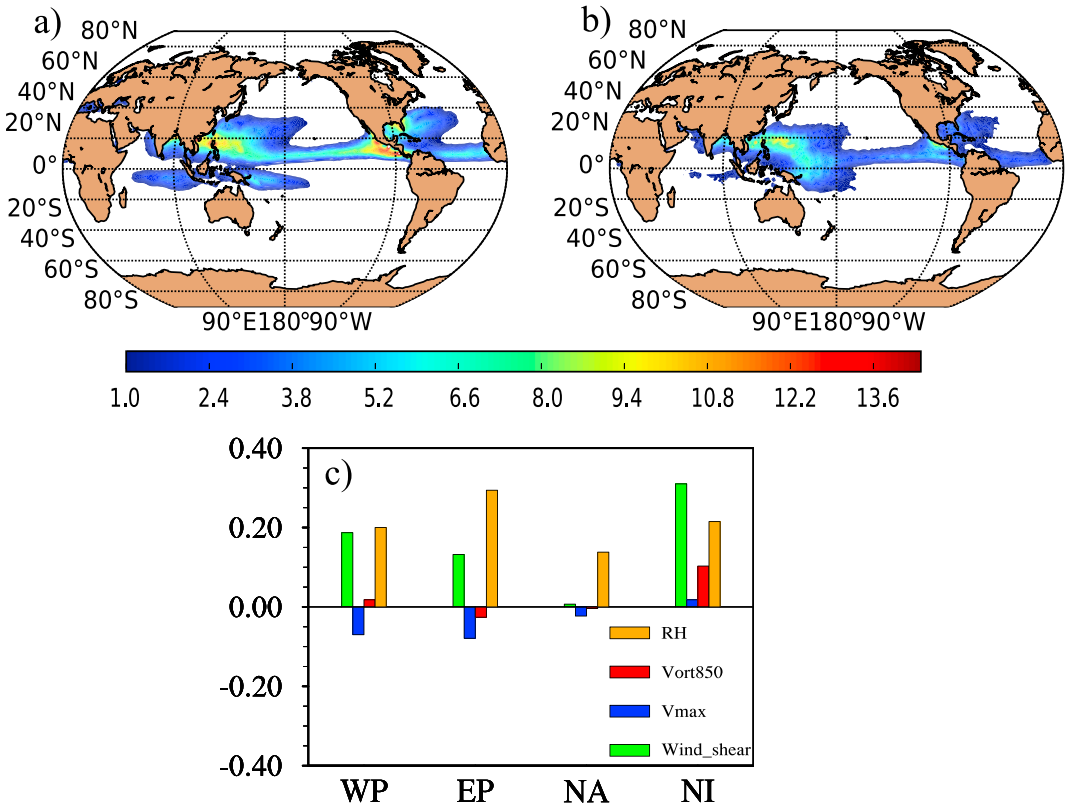

Figure 9. The tropical cyclone genesis potential index (GPI) in June–October (JJASO) during 1983–2002, based on ERA-interim (a) and FAMIL2 at C96 (~100 km) simulation (b). Panel (c) shows the biases of relative humidity (RH), absolute vorticity (vort850), maximum potential intensity (Vmax), and wind shear (Wind_shear) between 850 and 200 hPa in JJASO during 1983–2002 in the western Pacific (WP), eastern Pacific (EP), northern Atlantic (NA), and northern Indian Ocean (NI).

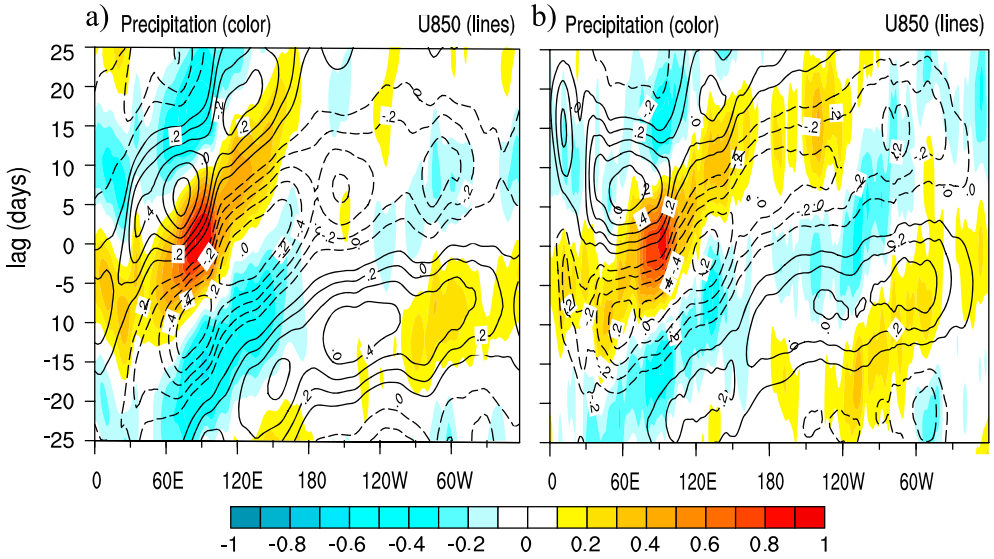

Figure 10. Comparison of annual (January–December) time-longitude diagrams for lag-composites of precipitation anomalies (color shading) and 850-hPa zonal wind between 10°S and 10°N in observation (a) and the FAMIL2 at C96 (~100 km) simulation (b) by using 20–100 band-pass-filtered data from 2001–2010. Color shading is for precipitation correlations, while the lagged correlations for the zonal winds are shown by the contours.

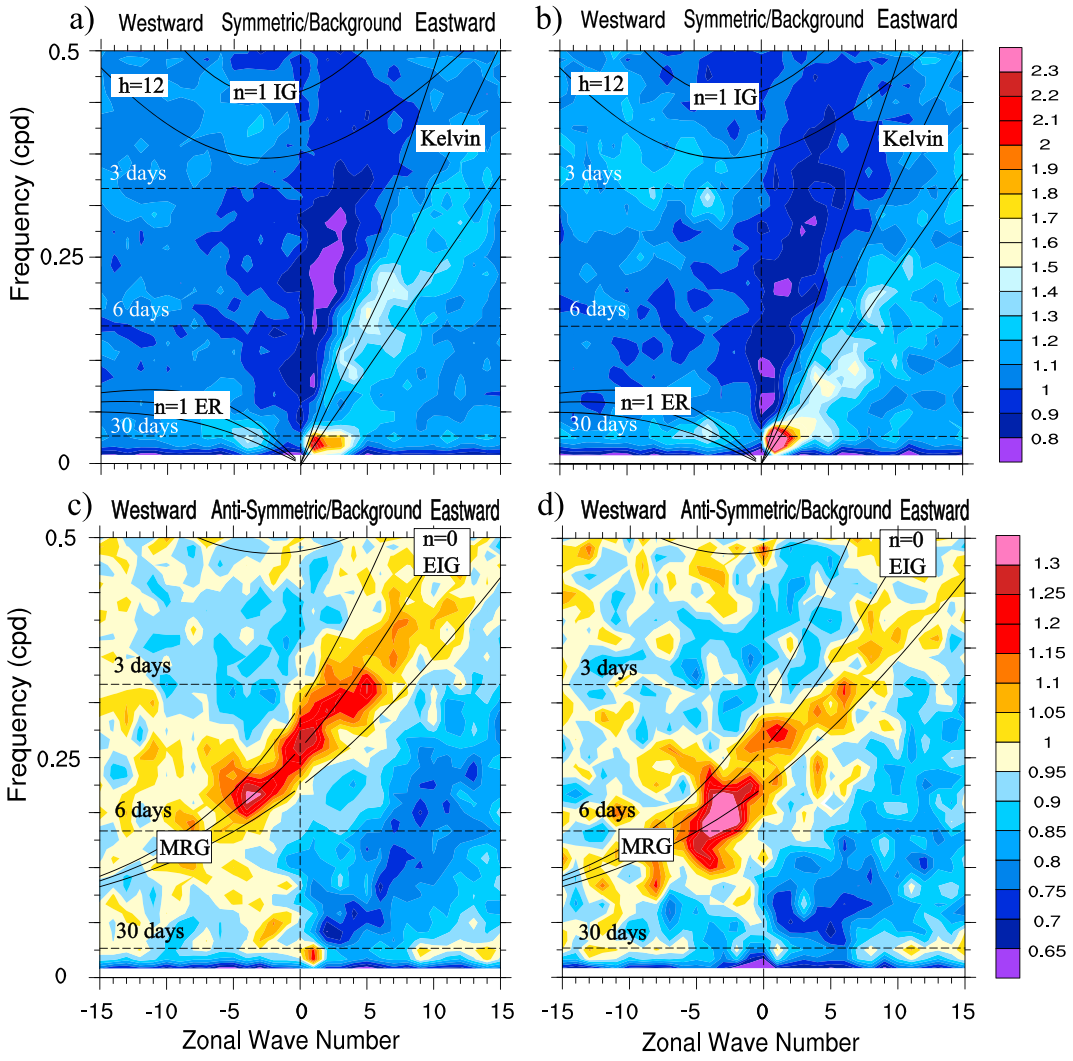

Figure 11. Space-time spectrum of the 15°S to 15°N symmetric (a, b) and antisymmetric (c, d) component of precipitation (shaded) divided by the background spectrum. The frequency spectral width is 1/128 cpd. Panels (a) and (c) are the observations, and panels (b) and (d) are the simulated results of FAMIL2 at the C96 (~100 km) resolution.

gravity, and mixed Rossby gravity modes for the three equivalent depths of 12, 15, and 50 m. It is obvious that there is an MJO signal in both the observation and simulation, the zonal wave numbers of which are 1–3 and the periodicities of which are 30–80 days. Although the signals, for example, the MJO and Kelvin wave, are stronger and narrower than observed, the CCEWs in their characteristic wave numbers are prominent. Therefore, the realistic simulation of the CCEWs and MJO provides a reasonable background for the genesis and propagation of TC.

6. Discussion

The impact of horizontal resolution on TC simulation has been widely studied, and some studies have pointed out the simulated performance of TC is improved when horizontal resolution is increased, (e.g., Manganello et al., 2012; Shaevitz et al., 2014; Strachan et al., 2013; Walsh et al., 2013). Figure 4 shows, the primary negative biases in TC numbers simulated by C96 (~100 km) FAMIL2 appear in the EP and NA. Also, Figure 12 (IBTrACS: Figure 12a; simulation: Figure 12b) shows that when the horizontal resolution is increased to C384 (~25 km), the percentage of TC in the EP increases from 6.7% to 16.4%, which is closer to the results in IBTrACS compared to the simulation in the C96 resolution. On the other hand, the total

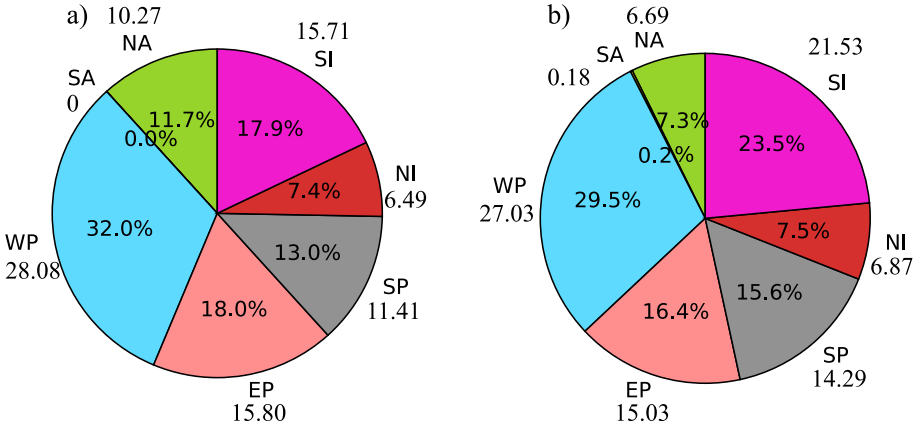

Figure 12. Comparison of the number of tropical cyclone in each basin in percentage terms between (a) IBTrACS and (b) FAMIL2 in C384 simulation (approximately 25 km) in the western Pacific (WP, blue), eastern Pacific (EP, pink), southern Pacific (SP, gray), northern Indian Ocean (NI, red), southern Indian Ocean (SI, purple), northern Atlantic (NA, green), and southern Atlantic (SA, yellow). The annually averaged tropical cyclone numbers are also shown in all basins.

percentage of TC in the WP is reduced from 10.4% to 2.5% compared to the results simulated at the C96 resolution. As for the intensity of TC (Figure 13), the simulation of C384 FAMIL2 exhibit a slightly enhanced compared with results from C96 FAMIL2, the "Category 3" hurricane can be detected in C384 FAMIL2 in an 8-year period of 1992–1999, while only "Category 1" hurricane is detected in C96 FAMIL2. By both regional and global model experiments, many studies claim nonhydrostatic dynamic core in a superhigh horizontal resolution plays a crucial role for the intensity of TC simulation. (e.g., Nakano et al., 2015, 2017; Satoh et al., 2014). Finally, the role the air-sea interaction as well as the model physics modules have been shown to be connected to the bias of the intensity and structure of TC simulation, especially the maximum wind speed (e.g., Mogensen et al., 2017; Srinivas et al., 2016; Zarzycki, 2016). Furthermore, several studies have discussed the impacts of physical processes, which include convective activity and cloud processes (e.g., Lin et al., 2006; Reed & Jablonowski, 2011a, 2011b; Stan, 2012; Zhang & McFarlane, 1995) on GCM-simulated climatology and variability of TC. Zhao et al. (2012) found that the simulation of TC genesis is sensitive to the cumulus mixing rate in a modified version of the convection scheme of Bretherton et al. (2004) and damping in the divergent component (Lin, 2004; Lin & Rood, 1997). Lim et al. (2015) found that the simulation of TC genesis, intensity, and 3-D structure is sensitive to the minimum entrainment of the modified version of the relaxed Arakawa–Schubert scheme (Moorthi & Suarez, 1992) in NASA's GEOS-5 model. Therefore, as for model development of FAMIL, a nonhydrostatic dynamic core in a high horizontal resolution (within 25 km), air-sea interaction as well as the model physics will be the potential future directions to further improve the skills of TC simulation.

The above analysis shows that C96 FAMIL2 exhibits reasonable performance in terms of the tracks, the numbers, and genesis locations of TC, especially over WP and NI regions. Therefore, we are in the process of setting up a seasonal TC forecasting system from the synoptic to seasonal time scale based on the coupled version of the model (Bao et al., 2018). Additionally, 1° horizontal resolution is quite cheap as to supercomputing resources and it shows a strong competitive ability so that we can easily design a reliable ensemble prediction system with a large ensemble.

7. Conclusion

In this study we have evaluated the performance of FAMIL2, at C96 (horizontal resolution of ~100 km), in simulating TC activity, focusing mainly on the climatology, variability, and intensity in the NIO, WP, and NA. The possible reasons behind the model's performance have been assessed with respect to the MJO, CCEWs, and the GPI. The main findings of the study can be summarized as follows:

1. At the C96 (~100 km) horizontal resolution, FAMIL2 can reasonably capture the main climatic patterns of the genesis locations, tracks, numbers, seasonal cycle, and intensity of TC. The main negative biases in TC numbers and tracks appear in the EP and NA. When the horizontal resolution is increased to C384

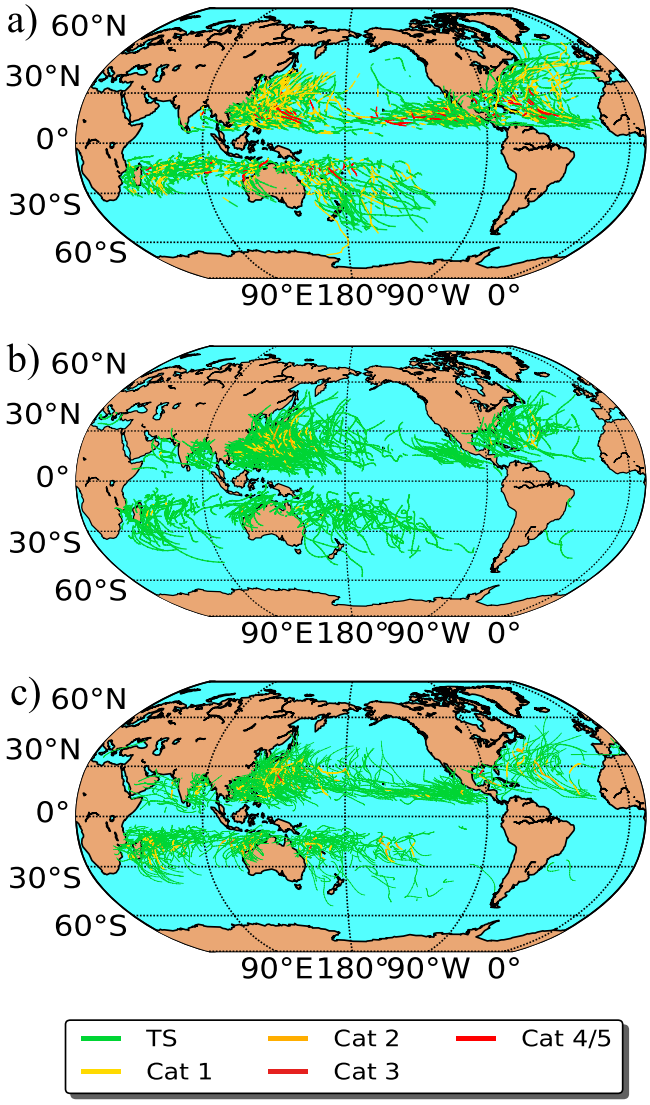

Figure 13. Tropical cyclone (TC) tracks (lines) and intensity (colors): (a) from an 8-year segment (1992–1999) of IBTrACS, (b) from an 8-year segment (1992–1999) simulation of FAMIL2 in C96 (~100 km), and (c) from an 8-year segment (1992–1999) simulation of FAMIL2 in C384 (approximately 25 km). The TC in FAMIL2 simulation are picked up by using an objective feature-tracking approach, and only those TC with a lifetime exceeding 3 days are shown. The TC in both the simulation of FAMIL2 and observation of IBTrACS are grouped into seven categories in accordance with the modified SS scale (Table 2), but only show the TC which intensities are stronger than "tropical storm" (TS).

(~25 km), the bias in TC numbers in the EP is reduced but the TC numbers in the NA do not increase obviously. A possible reason is the weaker easterly wave in the NA that goes against the genesis and propagation of TC. FAMIL2 can capture the main shape of the seasonal cycle in the NIO and WP, albeit with deficiencies in the detail. The main biases appear in the NA; only 60% of TC activity during the active season can be simulated, and the negative biases of TC numbers appear in the eastern part of NA that is near the northwest of Africa. One possible reason for the negative biases in TC numbers in NA is the weaker TC intensity compared to that of IBTrACS. When the TC intensity is weaker than IBTrACS, fewer TC events will be detected in NA. The intensities of TC simulated by FAMIL2 are weaker than those in IBTrACS. Moreover, there is no apparent improvement in the simulated intensities of TC when the horizontal resolution is increased from C96 (~100 km) to C384 (~25 km). According to the findings of other studies, there are many parameters to which the number and intensity of TC are sensitive. From the analysis of the GPI in each basin, the positive biases of relative humidity and wind

shear are the main hindrance to the accurate simulation of TC genesis. Meanwhile, the negative bias in maximum potential intensity, which is related to convective processes, is the main hindrance to an accurate simulation of the development of TC. It is necessary to carry out further research to identify the parameters and processes (Murakami et al., 2012) in FAMIL2 to which the model performance is sensitive.

2. In terms of the interannual variability of TC numbers, the correlation coefficients of 20-year TC numbers between FAMIL2 and IBTrACS is 0.22, 0.51 (95% confidence interval), and 0.49 (95% confidence interval) for the NIO, WP, and NA, respectively. Although the seasonal cycle and numbers in the NIO are close to those in IBTrACS, the correlation coefficients of 20-year TC numbers are lower than in the other basins. This reflects the difficulty for FAMIL2 in simulating the interannual variability in the NIO, which is an aspect that the next version of the model should address.
3. On the one hand, there are strong MJO and CCEW signals in the FAMIL2 simulation. Compared to observation, the spectral widths of these waves are narrower. For example, the zonal wave number of the MJO is from 1 to 5 in the observation, but only 1 to 3 in the simulation. Besides, the intensities of these waves are stronger than observed. On the other hand, the GPI is used to check the backgrounds contributing to TC genesis. The pattern of the GPI in FAMIL2 is close to ERA-Interim, but there are negative biases, particularly in the EP and NA, which are similar to the TC results by using the objective feature-tracking methodology.
4. Based on the performance of simulating TC, it is advisable to use this version of the model at the standard horizontal resolution (~100 km) when establishing a subseasonal to seasonal forecast system (Bao et al., 2018). Emanuel and Sobel (2013) discussed the importance of air-sea interaction for the genesis and maintenance of TCs, and indicated the deficiency in prescribing the SST for realistic TC simulation. Therefore, the subseasonal to seasonal forecast system should be a fully coupled version (MacLachlan et al., 2015; Yuan et al., 2011). Li et al. (2017) discussed the computational performance of FAMIL2 at different horizontal resolutions and with different CPU processes, and the result showed that the C96 (~100 km) resolution was computationally less expensive and the more efficient choice for FAMIL2. The seasonal forecasting skill (Camp et al., 2015; Manganello et al., 2016; Murakami et al., 2016; Xiang, Zhao, et al., 2015) with respect to TC in the WP, even in the Northern Hemisphere, will be discussed from the hindcast data set of a seasonal forecasting system based on FAMIL2 in the future.

Acknowledgments

This study was supported by funds from the National Key Research and Development Program Global Change and Mitigation Project (grant 2017YFA0604004) and the National Natural Science Foundation of China (grants 91737306, U1811464, 41675100, and 91637312). We thank the Editor and two anonymous reviewers for their careful review and constructive suggestions. ERA-Interim reanalysis observations were downloaded on the ECMWF website (http://apps.ecmwf.int/datasets/). TRMM 3B42 precipitation observations were downloaded on the NASA website (https://trmm.gsfc.nasa.gov/). OISSTv2 sea surface temperature observations were downloaded on the NOAA website (https://www.esrl.noaa.gov/psd/data/gridded/data.noaa.oisst.v2.highres.html). IBTrACS (v03r09) global tropical cyclone observations were downloaded on the NOAA website (https://www.ncdc.noaa.gov/ibtracs/). The FAMIL2 model outputs are available on request to B. Q. (baoqing@mail.iap.ac.cn).

References

Arakawa, A., & Schubert, W. H. (1974). Interaction of a cumulus cloud ensemble with the large-scale environment, part I. *Journal of the Atmospheric Sciences*, *31*(3), 674–701. https://doi.org/10.1175/1520-0469(1974)031<0674:IOACCE>2.0.CO;2

Banzon, V., Smith, T. M., Chin, T. M., Liu, C., & Hankins, W. (2016). A long-term record of blended satellite and in situ sea-surface temperature for climate monitoring, modeling and environmental studies. *Earth System Science Data*, *8*(1), 165–176. https://doi.org/10.5194/essd-8-165-2016

Bao, Q., Lin, P., Zhou, T., Liu, Y., Yu, Y., Wu, G., et al. (2013). The flexible global ocean-atmosphere-land system model, spectral version 2: FGOALS-s2. *Advances in Atmospheric Sciences*, *30*(3), 561–576. https://doi.org/10.1007/s00376-012-2113-9

Bao, Q., Wu, G., Liu, Y., Yang, J., Wang, Z., & Zhou, T. (2010). An introduction to the coupled model FGOALS1.1-s and its performance in East Asia. *Advances in Atmospheric Sciences*, *27*(5), 1131–1142. https://doi.org/10.1007/s00376-010-9177-1

Bao, Q., Wu, X., Li, J., Wang, L., He, B., Wang, X., et al. (2018). Outlook for El Niño and the Indian Ocean dipole in autumn-winter 2018–2019. *Chinese Science Bulletin*, *64*(1), 73–78.

Bender, M. A., Ginis, I., & Kurihara, Y. (1993). Numerical simulations of tropical cyclone-ocean interaction with a high-resolution coupled model. *Journal of Geophysical Research*, *98*(D12), 23,245–23,263. https://doi.org/10.1029/93JD02370

Bender, M. A., Ross, R. J., Tuleya, R. E., & Kurihara, Y. (1993). Improvements in tropical cyclone track and intensity forecasts using the GFDL initialization system. *Monthly Weather Review*, *121*(7), 2046–2061. https://doi.org/10.1175/1520-0493(1993)121<2046:IITCTA>2.0.CO;2

Bengtsson, L., Hodges, K. I., & Esch, M. (2007). Tropical cyclones in a T159 resolution global climate model: Comparison with observations and re-analyses. *Tellus Series A-dynamic Meteorology & Oceanography*, *59*(4), 396–416. https://doi.org/10.1111/j.1600-0870.2007.00236.x

Bretherton, C. S., McCaa, J. R., & Grenier, H. (2004). A new parameterization for shallow cumulus convection and its application to marine subtropical cloud-topped boundary layers. Part I: Description and 1D results. *Monthly Weather Review*, *132*(4), 864–882. https://doi.org/10.1175/1520-0493(2004)132<0864:ANPFSC>2.0.CO;2

Camargo, S. J., Emanuel, K. A., & Sobel, A. H. (2007). Use of a genesis potential index to diagnose ENSO effects on tropical cyclone genesis. *Journal of Climate*, *20*(19), 4819–4834. https://doi.org/10.1175/JCLI4282.1

Camp, J., Roberts, M., MacLachlan, C., Wallace, E., Hermanson, L., Brookshaw, A., et al. (2015). Seasonal forecasting of tropical storms using the Met Office GloSea5 seasonal forecast system. *Quarterly Journal of the Royal Meteorological Society*, *141*(691), 2206–2219. https://doi.org/10.1002/qj.2516

Caron, L.-P., Jones, C. G., & Winger, K. (2011). Impact of resolution and downscaling technique in simulating recent Atlantic tropical cylone activity. *Climate Dynamics*, *37*(5–6), 869–892. https://doi.org/10.1007/s00382-010-0846-7

Chen, J.-H., & Lin, S.-J. (2013). Seasonal predictions of tropical cyclones using a 25-km-resolution general circulation model. *Journal of Climate*, *26*(2), 380–398. https://doi.org/10.1175/JCLI-D-12-00061.1

Craig, A. P., Vertenstein, M., & Jacob, R. (2012). A new flexible coupler for earth system modeling developed for CCSM4 and CESM1. *The International Journal of High Performance Computing Applications*, *26*(1), 31–42. https://doi.org/10.1177/1094342011428141

CRED (2018). *Natural disasters 2017*. Brussels: CRED, 2018 EM-DAT file dated 02/07/2018. [available online at. https://cred.be/sites/default/files/adsr_2017.pdf

Dee, D., Uppala, S., Simmons, A., Berrisford, P., Poli, P., Kobayashi, S., et al. (2011). The ERA-interim reanalysis: Configuration and performance of the data assimilation system. *Quarterly Journal of the Royal Meteorological Society*, *137*(656), 553–597. https://doi.org/10.1002/qj.828

Emanuel, K. (1987). The dependence of hurricane intensity on climate. *Nature*, *326*(6112), 483–485. https://doi.org/10.1038/326483a0

Emanuel, K. (1995). Sensitivity of tropical cyclones to surface exchange coefficients and a revised steady-state model incorporating eye dynamics. *Journal of the Atmospheric Sciences*, *52*(22), 3969–3976.

Emanuel, K. (2005). Increasing destructiveness of tropical cyclones over the past 30 years. *Nature*, *436*(7051), 686–688. https://doi.org/10.1038/nature03906

Emanuel, K. (2017). Will global warming make hurricane forecasting more difficult? *Bulletin of the American Meteorological Society*, *98*(3), 495–501. https://doi.org/10.1175/BAMS-D-16-0134.1

Emanuel, K. & Nolan, D. S. (2004). Tropical Cyclone Activity and the Global Climate System.

Emanuel, K., & Sobel, A. (2013). Response of tropical sea surface temperature, precipitation, and tropical cyclone-related variables to changes in global and local forcing. *Journal of Advances in Modeling Earth Systems*, *5*, 447–458. https://doi.org/10.1002/jame.20032

Eyring, V., Bony, S., Meehl, G. A., Senior, C. A., Stevens, B., Stouffer, R. J., & Taylor, K. E. (2016). Overview of the Coupled Model Intercomparison Project Phase 6 (CMIP6) experimental design and organization. *Geoscientific Model Development*, *9*(5), 1937–1958. https://doi.org/10.5194/gmd-9-1937-2016

Fuentes-Franco, R., Giorgi, F., Coppola, E., & Zimmermann, K. (2017). Sensitivity of tropical cyclones to resolution, convection scheme and ocean flux parameterization over eastern tropical Pacific and tropical North Atlantic Oceans in the RegCM4 model. *Climate Dynamics*, *49*(1–2), 547–561. https://doi.org/10.1007/s00382-016-3357-3

Gates, W. L. (1992). AMIP: The atmospheric model intercomparison project. *Bulletin of the American Meteorological Society*, *73*(12), 1962–1970. https://doi.org/10.1175/1520-0477(1992)073<1962:ATAMIP>2.0.CO;2

Haarsma, R. J., Mitchell, J. F., & Senior, C. (1993). Tropical disturbances in a GCM. *Climate Dynamics*, *8*(5), 247–257. https://doi.org/10.1007/BF00198619

Haarsma, R. J., Roberts, M. J., Vidale, P. L., Senior, C. A., Bellucci, A., Bao, Q., et al. (2016). High resolution model intercomparison project (HighResMIP v1. 0) for CMIP6. *Geoscientific Model Development*, *9*(11), 4185–4208. https://doi.org/10.5194/gmd-9-4185-2016

Harris, L. M., & Lin, S.-J. (2014). Global-to-regional nested grid climate simulations in the GFDL high resolution atmospheric model. *Journal of Climate*, *27*(13), 4890–4910. https://doi.org/10.1175/JCLI-D-13-00596.1

Harris, L. M., Lin, S.-J., & Tu, C. (2016). High-resolution climate simulations using GFDL HiRAM with a stretched global grid. *Journal of Climate*, *29*(11), 4293–4314. https://doi.org/10.1175/JCLI-D-15-0389.1

Hartmann, D. L. (1994). *Global Physical Climatology*, X, (p. 411). N. Y: Academic Press.

Hodges, K. (1999). Adaptive constraints for feature tracking. *Monthly Weather Review*, *127*(6), 1362–1373. https://doi.org/10.1175/1520-0493(1999)127<1362:ACFFT>2.0.CO;2

Hodges, K. I. (1994). A general method for tracking analysis and its application to meteorological data. *Monthly Weather Review*, *122*(11), 2573–2586. https://doi.org/10.1175/1520-0493(1994)122<2573:AGMFTA>2.0.CO;2

Holtslag, A., & Boville, B. (1993). Local versus nonlocal boundary-layer diffusion in a global climate model. *Journal of Climate*, *6*(10), 1825–1842. https://doi.org/10.1175/1520-0442(1993)006<1825:LVNBLD>2.0.CO;2

Hung, M. P., Lin, J. L., Wang, W., Kim, D., Shinoda, T., & Weaver, S. J. (2013). MJO and convectively coupled equatorial waves simulated by CMIP5 climate models. *Journal of Climate*, *26*(17), 6185–6214. https://doi.org/10.1175/JCLI-D-12-00541.1

Jiang, X., Maloney, E. D., Li, J.-L. F., & Waliser, D. E. (2013). Simulations of the eastern North Pacific intraseasonal variability in CMIP5 GCMs. *Journal of Climate*, *26*(11), 3489–3510. https://doi.org/10.1175/JCLI-D-12-00526.1

Knapp, K. R., Kruk, M. C., Levinson, D. H., Diamond, H. J., & Neumann, C. J. (2010). The international best track archive for climate stewardship (IBTrACS) unifying tropical cyclone data. *Bulletin of the American Meteorological Society*, *91*(3), 363–376. https://doi.org/10.1175/2009BAMS2755.1

Knutson, T. R., McBride, J. L., Chan, J., Emanuel, K., Holland, G., Landsea, C., et al. (2010). Tropical cyclones and climate change. *Nature Geoscience*, *3*(3), 157–163. https://doi.org/10.1038/ngeo779

Knutson, T. R., Sirutis, J. J., Garner, S. T., Held, I. M., & Tuleya, R. E. (2007). Simulation of the recent multidecadal increase of Atlantic hurricane activity using an 18-km-grid regional model. *Bulletin of the American Meteorological Society*, *88*(10), 1549–1565. https://doi.org/10.1175/BAMS-88-10-1549

Korty, R. L., Camargo, S. J., & Galewsky, J. (2012). Variations in tropical cyclone genesis factors in simulations of the Holocene epoch. *Journal of Climate*, *25*(23), 8196–8211. https://doi.org/10.1175/JCLI-D-12-00033.1

Lamarque, J.-F., Emmons, L., Hess, P., Kinnison, D. E., Tilmes, S., Vitt, F., et al. (2012). CAM-chem: Description and evaluation of interactive atmospheric chemistry in the community earth system model. *Geoscientific Model Development*, *5*(2), 369–411. https://doi.org/10.5194/gmd-5-369-2012

Li, J., Bao, Q., Liu, Y., & Wu, G. (2017). Evaluation of the computational performance of the finite-volume atmospheric model of the IAP/LASG (FAMIL) on a high-performance computer. *Atmospheric and Oceanic Science Letters*, *10*(4), 329–336. https://doi.org/10.1080/16742834.2017.1331111

Lim, Y.-K., Schubert, S. D., Reale, O., Lee, M.-I., Molod, A. M., & Suarez, M. J. (2015). Sensitivity of tropical cyclones to parameterized convection in the NASA GEOS-5 model. *Journal of Climate*, *28*(2), 551–573. https://doi.org/10.1175/JCLI-D-14-00104.1

Lin, J. L., Kiladis, G. N., Mapes, B. E., Weickmann, K. M., Sperber, K. R., Lin, W., et al. (2006). Tropical Intraseasonal variability in 14 IPCC AR4 climate models. Part I: Convective signals. *Journal of Climate*, *19*(12), 2665–2690. https://doi.org/10.1175/JCLI3735.1

Lin, S.-J. (2004). A "vertically Lagrangian" finite-volume dynamical core for global models. *Monthly Weather Review*, *132*(10), 2293–2307. https://doi.org/10.1175/1520-0493(2004)132<2293:AVLFDC>2.0.CO;2

Lin, S. J., & Rood, R. B. (1997). An explicit flux-form semi-Lagrangian shallow-water model on the sphere. *Quarterly Journal of the Royal Meteorological Society*, *123*(544), 2477–2498. https://doi.org/10.1002/qj.49712354416

Lin, Y.-L., Farley, R. D., & Orville, H. D. (1983). Bulk parameterization of the snow field in a cloud model. *Journal of Climate and Applied Meteorology*, *22*(6), 1065–1092. https://doi.org/10.1175/1520-0450(1983)022<1065:BPOTSF>2.0.CO;2

MacLachlan, C., Arribas, A., Peterson, K., Maidens, A., Fereday, D., Scaife, A., et al. (2015). Global seasonal forecast system version 5 (GloSea5): A high-resolution seasonal forecast system. *Quarterly Journal of the Royal Meteorological Society*, *141*(689), 1072–1084. https://doi.org/10.1002/qj.2396

Manganello, J. V., Cash, B. A., Hodges, K. I. & Kinter, J. L. (2017). *Seasonal forecasts of North Atlantic tropical cyclone activity in the North American multi-model ensemble*, Climate Dynamics, Springer Berlin Heidelberg, 1-16.

Manganello, J. V., Hodges, K. I., Cash, B. A., Kinter, J. L. III, Altshuler, E. L., Fennessy, M. J., et al. (2016). Seasonal forecasts of tropical cyclone activity in a high-atmospheric-resolution coupled prediction system. *Journal of Climate*, *29*(3), 1179–1200. https://doi.org/10.1175/JCLI-D-15-0531.1

Manganello, J. V., Hodges, K. I., Kinter, J. L. III, Cash, B. A., Marx, L., Jung, T., et al. (2012). Tropical cyclone climatology in a 10-km global atmospheric GCM: Toward weather-resolving climate modeling. *Journal of Climate*, *25*(11), 3867–3893. https://doi.org/10.1175/JCLI-D-11-00346.1

Meinshausen, M., Smith, S. J., Calvin, K., Daniel, J. S., Kainuma, M., Lamarque, J.-F., et al. (2011). The RCP greenhouse gas concentrations and their extensions from 1765 to 2300. *Climatic Change*, *109*(1–2), 213–241. https://doi.org/10.1007/s10584-011-0156-z

Mendelsohn, R., Emanuel, K., Chonabayashi, S., & Bakkensen, L. (2012). The impact of climate change on global tropical cyclone damage. *Nature Climate Change*, *2*(3), 205–209. https://doi.org/10.1038/nclimate1357

Mogensen, K. S., Magnusson, L., & Bidlot, J. R. (2017). Tropical cyclone sensitivity to ocean coupling in the ECMWF coupled model. *Journal of Geophysical Research: Oceans*, *122*, 4392–4412. https://doi.org/10.1002/2017JC012753

Moorthi, S., & Suarez, M. J. (1992). Relaxed Arakawa-Schubert. A parameterization of moist convection for general circulation models. *Monthly Weather Review*, *120*(6), 978–1002. https://doi.org/10.1175/1520-0493(1992)120<0978:RASAPO>2.0.CO;2

Murakami, H., Vecchi, G. A., Villarini, G., Delworth, T. L., Gudgel, R., Underwood, S., et al. (2016). Seasonal forecasts of major hurricanes and landfalling tropical cyclones using a high-resolution GFDL coupled climate model. *Journal of Climate*, *29*(22), 7977–7989. https://doi.org/10.1175/JCLI-D-16-0233.1

Murakami, H., Wang, B., & Kitoh, A. (2011). Future change of western North Pacific typhoons: Projections by a 20-km-mesh global atmospheric model. *Journal of Climate*, *24*(4), 1154–1169. https://doi.org/10.1175/2010JCLI3723.1

Murakami, H., Wang, Y., Yoshimura, H., Mizuta, R., Sugi, M., Shindo, E., et al. (2012). Future changes in tropical cyclone activity projected by the new high-resolution MRI-AGCM. *Journal of Climate*, *25*(9), 3237–3260. https://doi.org/10.1175/JCLI-D-11-00415.1

Nakano, M., Sawada, M., Nasuno, T., & Satoh, M. (2015). Intraseasonal variability and tropical cyclogenesis in the western North Pacific simulated by a global nonhydrostatic atmospheric model. *Geophysical Research Letters*, *42*, 565–571. https://doi.org/10.1002/2014GL062479

Nakano, M., Wada, A., Sawada, M., Yoshimura, H., Onishi, R., Kawahara, S., et al. (2017). Global 7 km mesh nonhydrostatic model intercomparison project for improving TYphoon forecast (TYMIP-G7): Experimental design and preliminary results. *Geoscientific Model Development*, *10*(3), 1363–1381. https://doi.org/10.5194/gmd-10-1363-2017

Oleson, K. W., Lawrence, D. M., Gordon, B., Flanner, M. G., Kluzek, E., Peter, J., et al. (2010). Technical description of version 4.0 of the community land model (CLM).

Oouchi, K., Noda, A. T., Satoh, M., Miura, H., Tomita, H., Nasuno, T., & Iga, S. I. (2009). A simulated preconditioning of typhoon genesis controlled by a boreal summer Madden-Julian Oscillation event in a global cloud-system-resolving model. *Sola*, *5*, 65–68. https://doi.org/10.2151/sola.2009-017

Oouchi, K., Yoshimura, J., Yoshimura, H., Mizuta, R., Kusunoki, S., & Noda, A. (2006). Tropical cyclone climatology in a global-warming climate as simulated in a 20 km-mesh global atmospheric model: Frequency and wind intensity analyses. *Journal of the Meteorological Society of Japan Ser. II*, *84*(2), 259–276. https://doi.org/10.2151/jmsj.84.259

Park, S., & Bretherton, C. S. (2009). The University of Washington shallow convection and moist turbulence schemes and their impact on climate simulations with the community atmosphere model. *Journal of Climate*, *22*(12), 3449–3469. https://doi.org/10.1175/2008JCLI2557.1

Peters, K., Crueger, T., Jakob, C., & Möbis, B. (2017). Improved MJO-simulation in ECHAM6. 3 by coupling a stochastic multicloud model to the convection scheme. *Journal of Advances in Modeling Earth Systems*, *9*, 193–219. https://doi.org/10.1002/2016MS000809

Putman, W. M., & Lin, S.-J. (2007). Finite-volume transport on various cubed-sphere grids. *Journal of Computational Physics*, *227*(1), 55–78. https://doi.org/10.1016/j.jcp.2007.07.022

Reed, K. A., & Jablonowski, C. (2011a). Impact of physical parameterizations on idealized tropical cyclones in the Community Atmosphere Model. *Geophysical Research Letters*, *38*, L04805. https://doi.org/10.1029/2010GL046297

Reed, K. A., & Jablonowski, C. (2011b). Assessing the uncertainty in tropical cyclone simulations in NCAR's community atmosphere model. *Journal of Advances in Modeling Earth Systems*, *3*, M08002. https://doi.org/10.1029/2011MS000076

Reynolds, R. W., Smith, T. M., Liu, C., Chelton, D. B., Casey, K. S., & Schlax, M. G. (2007). Daily high-resolution-blended analyses for sea surface temperature. *Journal of Climate*, *20*(22), 5473–5496. https://doi.org/10.1175/2007JCLI1824.1

Royer, J. F., Chauvin, F., Timbal, B., Araspin, P., & Grimal, D. (1998). A GCM study of the impact of greenhouse gas increase on the frequency of occurrence of tropical cyclones. *Climatic Change*, *38*(3), 307–343. https://doi.org/10.1023/A:1005386312622

Satoh, M., Tomita, H., Yashiro, H., Miura, H., Kodama, C., Seiki, T., et al. (2014). The non-hydrostatic icosahedral atmospheric model: Description and development. *Progress in Earth and Planetary Science*, *1*(1), 18. https://doi.org/10.1186/s40645-014-0018-1

Shaevitz, D. A., Camargo, S. J., Sobel, A. H., Jonas, J. A., Kim, D., Kumar, A., et al. (2014). Characteristics of tropical cyclones in high-resolution models in the present climate. *Journal of Advances in Modeling Earth Systems*, *6*, 1154–1172. https://doi.org/10.1002/2014MS000372

Shen, W., Tang, J., Wang, Y., Wang, S., & Niu, X. (2017). Evaluation of WRF model simulations of tropical cyclones in the western North Pacific over the CORDEX East Asia domain. *Climate Dynamics*, *48*(7–8), 2419–2435. https://doi.org/10.1007/s00382-016-3213-5

Shepherd, T. J., & Walsh, K. J. (2016). Sensitivity of hurricane track to cumulus parameterization schemes in the WRF model for three intense tropical cyclones: Impact of convective asymmetry. *Meteorology and Atmospheric Physics*, *129*(4), 345–374. https://doi.org/10.1007/s00703-016-0472-y

Simpson, R. H., & Saffir, H. (1974). The hurricane disaster potential scale. *Weatherwise*, *27*(8), 169.

Small, R. J., Bacmeister, J., Bailey, D., Baker, A., Bishop, S., Bryan, F., et al. (2014). A new synoptic scale resolving global climate simulation using the Community Earth System Model. *Journal of Advances in Modeling Earth Systems*, *6*, 1065–1094. https://doi.org/10.1002/2014MS000363

Srinivas, C., Mohan, G. M., Naidu, C., Baskaran, R., & Venkatraman, B. (2016). Impact of air-sea coupling on the simulation of tropical cyclones in the North Indian Ocean using a simple 3-D ocean model coupled to ARW. *Journal of Geophysical Research: Atmospheres*, *121*, 9400–9421. https://doi.org/10.1002/2015JD024431

Stan, C. (2012). Is cumulus convection the concertmaster of tropical cyclone activity in the Atlantic? *Geophysical Research Letters*, *39*, L19716. https://doi.org/10.1029/2012GL053449

Strachan, J., Vidale, P. L., Hodges, K., Roberts, M., & Demory, M.-E. (2013). Investigating global tropical cyclone activity with a hierarchy of AGCMs: The role of model resolution. *Journal of Climate*, *26*(1), 133–152. https://doi.org/10.1175/JCLI-D-12-00012.1

Tao, D., & Zhang, F. (2014). Effect of environmental shear, sea-surface temperature, and ambient moisture on the formation and predictability of tropical cyclones: An ensemble-mean perspective. *Journal of Advances in Modeling Earth Systems*, *6*, 384–404. https://doi.org/10.1002/2014MS000314

Voosen, P. (2017). The weather master. *American Association for the Advancement of Science*, *356*(6334), 128–131. https://doi.org/10.1126/science.356.6334.128

Waliser, D., Sperber, K., Hendon, H., Kim, D., Maloney, E., Wheeler, M., et al. (2009). MJO simulation diagnostics. *Journal of Climate*, *22*(11), 3006–3030.

Walsh, K., Camargo, S., Vecchi, G., Daloz, A., Elsner, J., Emanuel, K., et al. (2015). Hurricanes and climate: The US CLIVAR working group on hurricanes. *Bulletin of the American Meteorological Society*, *96*(6), 997–1017. https://doi.org/10.1175/BAMS-D-13-00242.1

Walsh, K., Lavender, S., Scoccimarro, E., & Murakami, H. (2013). Resolution dependence of tropical cyclone formation in CMIP3 and finer resolution models. *Climate dynamics*, *40*(3-4), 585–599.

Walsh, K. J. E., Fiorino, M., Landsea, C. W., & Mcinnes, K. L. (2007). Objectively determined resolution-dependent threshold criteria for the detection of tropical cyclones in climate models and reanalyses. *Journal of Climate*, *20*(10), 2307–2314. https://doi.org/10.1175/JCLI4074.1

Wang, X., Liu, Y., Wu, G., Lin, S.-J., & Bao, Q. (2013). The application of flux-form semi-Lagrangian transport scheme in a spectral atmosphere model. *Advances in Atmospheric Sciences*, *30*(1), 89–100. https://doi.org/10.1007/s00376-012-2039-2

Wheeler, M., & Kiladis, G. N. (2010). Convectively coupled equatorial waves: Analysis of clouds and temperature in the wavenumber-frequency domain. *Journal of the Atmospheric Sciences*, *56*(3), 374–399.

Wu, G., & Lau, N. C. (1992). A GCM simulation of the relationship between tropical-storm formation and ENSO. *Monthly Weather Review*, *12*(6), 958–977.

Xiang, B., Lin, S.-J., Zhao, M., Zhang, S., Vecchi, G., Li, T., et al. (2015). Beyond weather time-scale prediction for Hurricane Sandy and super Typhoon Haiyan in a global climate model. *Monthly Weather Review*, *143*(2), 524–535. https://doi.org/10.1175/MWR-D-14-00227.1

Xiang, B., Zhao, M., Jiang, X., Lin, S.-J., Li, T., Fu, X., & Vecchi, G. (2015). The 3–4-week MJO prediction skill in a GFDL coupled model. *Journal of Climate*, *28*(13), 5351–5364. https://doi.org/10.1175/JCLI-D-15-0102.1

Ying, M., Zhang, W., Yu, H., Lu, X., Feng, J., Fan, Y., et al. (2014). An overview of the China Meteorological Administration tropical cyclone database. *Journal of Atmospheric & Oceanic Technology*, *31*(2), 287–301. https://doi.org/10.1175/JTECH-D-12-00119.1

Yuan, X., Wood, E. F., Luo, L., & Pan, M. (2011). A first look at climate forecast system version 2 (CFSv2) for hydrological seasonal prediction. *Geophysical Research Letters*, *38*, L13402. https://doi.org/10.1029/2011GL047792

Zarzycki, C. M. (2016). Tropical cyclone intensity errors associated with lack of two-way ocean coupling in high-resolution global simulations. *Journal of Climate*, *29*(23), 8589–8610. https://doi.org/10.1175/JCLI-D-16-0273.1

Zarzycki, C. M., & Jablonowski, C. (2014). A multidecadal simulation of Atlantic tropical cyclones using a variable-resolution global atmospheric general circulation model. *Journal of Advances in Modeling Earth Systems*, *6*, 805–828. https://doi.org/10.1002/2014MS000352

Zhang, C. (2005). Madden-Julian oscillation. *Reviews of Geophysics*, *43*, RG2003. https://doi.org/10.1029/2004RG000158

Zhang, C. (2013). Madden–Julian oscillation: Bridging weather and climate. *Bulletin of the American Meteorological Society*, *94*(12), 1849–1870. https://doi.org/10.1175/BAMS-D-12-00026.1

Zhang, G. J., & McFarlane, N. A. (1995). Sensitivity of climate simulations to the parameterization of cumulus convection in the Canadian Climate Centre general circulation model. *Atmosphere-Ocean*, *33*(3), 407–446. https://doi.org/10.1080/07055900.1995.9649539

Zhao, M., Held, I. M., & Lin, S.-J. (2012). Some counterintuitive dependencies of tropical cyclone frequency on parameters in a GCM. *Journal of the Atmospheric Sciences*, *69*(7), 2272–2283. https://doi.org/10.1175/JAS-D-11-0238.1

Zhao, M., Held, I. M., Lin, S.-J., & Vecchi, G. A. (2009). Simulations of global hurricane climatology, interannual variability, and response to global warming using a 50-km resolution GCM. *Journal of Climate*, *22*(24), 6653–6678. https://doi.org/10.1175/2009JCLI3049.1

Zhou, L., Bao, Q., Liu, Y., Wu, G., Wang, W. C., Wang, X., et al. (2015). Global energy and water balance: Characteristics from finite-volume atmospheric model of the IAP/LASG (FAMIL1). *Journal of Advances in Modeling Earth Systems*, *7*, 1–20. https://doi.org/10.1002/2014MS000349

Zhou, L., Liu, Y., Bao, Q., Yu, H., & Wu, G. (2012). Computational performance of the high-resolution atmospheric model FAMIL. *Atmospheric and Oceanic Science Letters*, *5*(5), 355–359.